NASA MEMO 1-19-59L

NASA

MEMORANDUM

TRAJECTORY CONTROL FOR VEHICLES ENTERING THE EARTH'S ATMOSPHERE AT SMALL FLIGHT-PATH ANGLES

By John M. Eggleston and John W. Young

Langley Research Center
Langley Field, Va.

NATIONAL AERONAUTICS AND SPACE ADMINISTRATION

WASHINGTON

February 1959

Declassified December 1, 1959

NATIONAL AERONAUTICS AND SPACE ADMINISTRATION

MEMORANDUM 1-19-59L

TRAJECTORY CONTROL FOR VEHICLES ENTERING THE EARTH'S ATMOSPHERE AT SMALL FLIGHT-PATH ANGLES*

By John M. Eggleston and John W. Young

SUMMARY

Methods of controlling the trajectories of high-drag—low-lift vehicles entering the earth's atmosphere at angles of attack near 90° and at initial entry angles up to 3° are studied. The trajectories are calculated for vehicles whose angle of attack can be held constant at some specified value or can be perfectly controlled as a function of some measured quantity along the trajectory. The results might be applied in the design of automatic control systems or in the design of instruments which will give the human pilot sufficient information to control his trajectory properly during an atmospheric entry.

Trajectory data are compared on the basis of the deceleration, range, angle of attack, and, in some cases, the rate of descent. The aerodynamic heat-transfer rate and skin temperature of a vehicle with a simple heat-sink type of structure are calculated for trajectories made with several types of control functions.

For the range of entry angles considered, it is found that the angle of attack can be controlled to restrict the deceleration down to an arbitrarily chosen level of 3g. All the control functions tried are successful in reducing the maximum deceleration to the desired level. However, in order to avoid a tendency for the deceleration to reach an initial peak, decrease, and then reach a second peak, some anticipation is required in the control function so that the change in angle of attack will lead the change in deceleration. When the angle of attack is controlled in the aforementioned manner, the maximum rate of aerodynamic heat transfer to the skin is reduced, the maximum skin temperature of the vehicle is virtually unaffected, and the total heat absorbed is slightly increased. The increase in total heat can be minimized, however, by maintaining the maximum desired deceleration for as much of the trajectory as possible. From an initial angle of attack of 90°, the angle-of-attack requirements necessary to maintain constant values of deceleration (1g to 4g) and constant values of rate of descent (450 to 1,130 ft/sec) as long as it is aerodynamically practical are calculated and are found to be moderate in both magnitude and rate. Entry trajectories made with these types of control are presented and discussed.

*Title, Unclassified.

INTRODUCTION

For the successful recovery of satellite and near-satellite vehicles it is generally necessary to maintain deceleration and heating within certain limiting values. In addition, it is desirable to be able to predict with reasonable accuracy the trajectory and range of the vehicle. A logical means of achieving these objectives is to control the trajectory by varying the aerodynamic forces generated during entry into the atmosphere.

At present, the National Aeronautics and Space Administration and other research agencies are investigating factors important to the development of satellite vehicles as well as a number of general satellite configurations which hold promise of achieving desirable and predictable conditions during their return to earth. This paper deals with the control of the point-mass trajectories through the earth's atmosphere of one general class of space vehicles, namely, vehicles which have a large flat-plate area which is maintained nearly normal to its flight path during most of the entry. This class of vehicles includes circular- or delta-wing gliders as well as capsules having blunted faces. Methods of controlling the deceleration and trajectory include either varying or maintaining constant the angle of attack in the range near 90°. By maintaining the angle of attack near 90°, a strong detached shock wave is produced ahead of the vehicle which in turn dissipates a large percentage of the energy into the atmosphere with a consequent lower heat transfer to the vehicle itself. By changing or maintaining the angle of attack to values smaller than 90°, a component of the resultant aerodynamic force is produced normal to the flight path. This lifting force reduces the rate of descent into the denser atmosphere and consequently the deceleration and heating that would result in this denser atmosphere.

The first consideration, that of maintaining a large ratio of wave drag to friction drag, is an important result reported by Allen and Eggers in reference 1. The second consideration which involves the production of small lift-drag ratios to control point-mass trajectories has been widely recognized as a most logical approach to trajectory control. Some of the effects of a small constant lift-drag ratio during atmospheric entries are given in reference 2. The purpose of this paper is to utilize these concepts and to determine the effects of controlling the angle of attack, and hence the lift, as a function of the measurable trajectory variables in such a manner as to achieve low levels of deceleration which will not incapacitate a human pilot and to minimize the increase in the total temperature and the range compared with that of the zero-lift case for the same vehicle. The results might be applied in the design of automatic control systems or in the design of instruments which would give the human pilot sufficient information to

control his trajectory properly during the entry. As an aid in achieving these ends, studies are also made of families of trajectories in which the angle of attack is varied to maintain one of the flight variables constant, namely, either deceleration or rate of descent.

Although the assumptions used in the trajectory calculations are believed to be adequate to provide quantitative results, the calculations of temperatures are only qualitative since the temperature over the surface of the vehicle will depend on many specialized factors of design and material.

SYMBOLS

a_n	deceleration in direction of resultant aerodynamic force, $-a_z$
a_v	component of deceleration along flight path, $\dot{V}/g$
a_z	deceleration along Z-axis of vehicle
c	speed of sound, $(dp/d\rho)^{1/2}_{\text{isentropic}}$
C	heat capacity of material
C_F	aerodynamic force coefficient, $2F/\rho V^2 S$
D	drag, $F \sin \alpha$
F	resultant aerodynamic force
g	acceleration due to gravity
h	radial height above surface of earth, $r - r_e$
H	constant for exponential variation of density
k	emissivity-absorptivity factor
K_1	variation of angle of attack with deceleration (see eq. (20))
K_2	variation of angle of attack with rate of change in deceleration (see eq. 21))
K_3	variation of angle of attack with temperature

L	lift, $F \cos \alpha$
m	mass of vehicle, W/g
M	Mach number, V/c
p	free-stream pressure
q	free-stream dynamic pressure, $\frac{1}{2}\rho V^2$
Q/A	heat-flow rate per unit area
r	radial distance measured from geographical center of earth
r*	effective radius of total surface area of vehicle normal to flow, $\sqrt{S/\pi}$
R	perfect gas constant for air
Δs	perimetric distance over surface of earth traversed since zero time (range)
S	frontal area of vehicle (assumed to be equivalent to wing area)
t	time
T	free-stream temperature
T_1	vehicle skin temperature based on W_1C/A of 0.8
T_1*	vehicle skin temperature based on W_1C/A of 0.2
T_2	radiation equilibrium temperature
V	free-stream velocity
V_t	tangential velocity, component of total velocity normal to radial vector
W	weight of vehicle
W/S	wing loading of vehicle
W_1/A	weight per unit surface area of vehicle skin material
X	vehicle body axis alined with wing-chord plane

Z	vehicle body axis normal to wing-chord plane
α	angle of attack
$\beta(t)$	an explicit function of time used in appendix A
γ	flight-path angle
γ_o	initial flight-path angle, entry angle
γ_1	ratio of specific heats for air
δ	angle between velocity vector and reference horizon
Θ	angle between reference horizon and tangential velocity, angular rotation of radial vector to point mass
ξ_1, ξ_2	temperature constants
ρ	free-stream density
ρ_e	constant for exponential variation of density
σ	Stefan-Boltzmann constant for radiation

Symbols used only in appendix C:

a_θ	horizontal component of deceleration
u	horizontal component of velocity

$\bar{u} = u/\sqrt{gr} \cong V/\sqrt{gr}$

Z	nondimensional parameter of reference 2

$\beta \equiv 1/H$

$\varphi \equiv \gamma$

$\Delta( ) = ( )_n - ( )_{n-1}$

Subscripts:

o	initial condition, that is, value at zero time
e	referenced to mean surface of earth
d	design

Derivatives with respect to time are denoted with dots over the variable. For example, $d\gamma/dt = \dot{\gamma}$.

EQUATIONS OF MOTION

This study is concerned with entry into the earth's atmosphere of a vehicle which is traveling at or near the velocity of 26,000 feet per second and is entering the atmosphere on a flight path which initially differs from the instantaneous horizon by a small angle $(-\gamma)$ not exceeding 3°. On the basis of current knowledge of the atmosphere the trajectory studies were started at an initial altitude of 350,000 feet. It is assumed that above this altitude the effect of the atmosphere on the flight path is negligible.[1] A schematic diagram of a typical trajectory showing this initial condition is shown in figure 1. The forces, acceleration, velocities, and displacements are shown in their positive sense except as noted.

The vehicle considered in this study is assumed to have a large flat-plate area such as a wing which is stabilized nearly normal to the flight path (that is, at an angle of attack of nearly 90°) at the time of the initial conditions. It is further assumed that this angle of attack may be maintained at a constant value or changed without lag to any desired value during its trajectory within the atmosphere. The resulting motions are assumed to be those of a point mass and no moment equation is included in the equations of motion.

The governing equations of motion, when the notation of figure 1 is used, are as follows:

$$\left.\begin{aligned} m\dot{V} &= -D - W \sin \gamma \\ mV\dot{\delta} &= L - W \cos \gamma \\ \dot{h} &= V \sin \gamma \\ \dot{\Theta} &= \frac{V}{r} \cos \gamma \end{aligned}\right\} \tag{1}$$

For the relatively small values of altitude covered, the acceleration due to gravity and the distance from the vehicle to the center of the earth are assumed to be constant; that is,

---

[1]The effect of the atmosphere on vehicle temperatures at these altitudes however is not negligible. (See the section entitled "Temperature Equilibrium Equations.")

$$g = 32.2 \text{ ft/sec}^2$$

$$gr = 25{,}863 \text{ ft/sec}$$

An exponential variation of density with altitude is used such that

$$\rho(h) = \rho_e e^{-h/H} \tag{2}$$

with

$$\rho_e = 0.003$$

$$H = 23{,}000 \text{ ft}$$

Newtonian flow is assumed at the surface of the flat-plate area during the entire trajectory although this assumption will undoubtedly be violated during the final stages of the trajectory where the velocity falls below 5,000 feet per second. Accordingly, a force

$$F = \frac{1}{2}\rho V^2 S C_F = -mga_z \tag{3}$$

is assumed to act normal to the flat-plate area at all times. The components of this force along and normal to the flight path are denoted as the drag

$$D(\alpha) = F \sin \alpha \tag{4}$$

and the lift

$$L(\alpha) = F \cos \alpha \tag{5}$$

in the usual sense. A value for the aerodynamic-force coefficient normal to the plate was chosen as

$$C_{F'} = 1.7$$

and was assumed to be invariant with angle of attack over the range of conditions covered. This value of C_F is slightly less than the pure Newtonian pressure coefficient of 2.0 and slightly greater than the (asymptotic) value of about 1.6 which is predicted for the pressure coefficient on a cone of maximum apex angle for an attached shock at hypersonic Mach numbers. (See ref. 3.)

The variable δ is related to Θ and γ by

$$\delta = \gamma - \Theta \tag{6}$$

as defined by the sign convention of figure 1. By substituting equations (2) to (6) into equations (1), the equations of motion may be written as follows:

$$\left.\begin{aligned} \frac{\dot{V}}{g} &= -a_n \sin\alpha - \sin\gamma \\ \frac{V\dot{\gamma}}{g} &= a_n \cos\alpha + \left(\frac{V^2}{gr} - 1\right)\cos\gamma \\ \dot{h} &= V \sin\gamma \end{aligned}\right\} \tag{7}$$

$$a_n = -a_z = \left(\frac{\rho_e C_F}{2W/S}\right) e^{-h/H} V^2 \tag{8}$$

where a_n is the acceleration measured normal to the flat plate, as is shown in figure 1.

The range on the surface of the earth is given by the integral

$$\Delta s = r_e \int_0^{\Theta(t)} d\Theta = r_e \int_0^t \frac{V}{r} \cos\gamma \, dt \tag{9}$$

Since r was assumed to be constant and equal to r_e, no distinction is made between the range on the surface of the earth and that at altitude h.

When the angle of attack and the three initial conditions are specified, equations (7) to (9) define the trajectory from these initial

conditions. Another type of solution may be found when some variable or combination of variables other than angle of attack is specified and the equations are solved for the variation in angle of attack necessary to produce this condition. Both types of solutions are investigated in subsequent sections.

TEMPERATURE EQUILIBRIUM EQUATIONS

For the trajectories where temperature calculations are presented, a simple model was used to represent a unit area of the exposed surface of the vehicle. The rate of heat flow into the material from the boundary layer was calculated by using an expression derived in reference 4 for the stagnation point of a rounded blunt body. This expression, given in units of Btu/sec-ft^2, is

$$\left(\frac{Q}{A}\right)_{\text{aerodynamic}} = 0.010M^{3.1}\left(\frac{p}{r^*}\right)^{0.5} \tag{10}$$

where the constant 0.010 is determined by the roundness of the surface, r^* is the effective radius of the total surface area normal to the flow, and p and M are, respectively, the free-stream static pressure and Mach number. The constant 0.010 is somewhat less than the value used by Romig since it is assumed that the curvature of the undersurface of the vehicle is less rounded than that of the model used by Romig. The value of r^* was taken as 8 feet which corresponds to a vehicle flat-plate area of 200 square feet.

The net rate of heat transfer by radiation from the surface at a temperature T_1 to the surroundings at temperature T_2 was calculated from the expression:

$$\left(\frac{Q}{A}\right)_{\text{radiation}} = k\sigma\left(T_1^4 - T_2^4\right) \tag{11}$$

where σ is the Stefan-Boltzmann constant, 0.48×10^{-12} $\frac{\text{Btu}}{\text{ft}^2\text{-sec-}^\circ\text{R}^4}$ and k is the emissivity-absorptivity factor. Unpublished calculations and measurements indicate that at an altitude of about 100 miles the radiation equilibrium temperature between the surface and the surroundings will be about 580° R. Since the calculated aerodynamic heating rate (based on the assumed model atmosphere) is negligible at this altitude, the initial equilibrium temperature of the vehicle will also be about 580° R.

It was assumed that the surface radiated from only one side but at an effectiveness of unity (k = 1.0). The result of the two assumptions is more realistic than the results with either assumption singly.

The heat absorbed by the structure is dependent on the product of the weight per unit area and the heat capacity of the material used. For the calculations herein, the rate of heat absorbed per unit area

$$\frac{W_1 C}{A} \dot{T}_1 \tag{12}$$

was calculated for 1/8-inch solid beryllium such that

$$\frac{W_1}{A} = 1.1844 \text{ lb/sq ft}$$

$$C = 0.675 \frac{\text{Btu}}{\text{lb-}^{\circ}\text{R}}$$

The product $\frac{W_1 C}{A}$ is thus 0.8. In some cases[2] the material was considered to have less heat capacity (for example, a thinner gage material) and the product of the two terms was reduced to 0.2. However, unless otherwise specified, the value 0.8 was used in all temperature calculations.

A third element of heat transport, conduction between the skin material and the internal structure, is neglected in these calculations. One further simplification is employed by assuming that this unit area of material is always located at the stagnation point (or region) of the vehicle's surface in spite of the fact that the angle of attack is being varied. Some justification for this assumption may be found in reference 5.

The heat capacity of the material together with the two elements of heat transport considered, namely, conduction from the boundary layer to the material and radiation between the material and its surroundings, constitute a balance within the chosen control surface. Thus,

---

[2]For the purposes of this paper, the material need not be an integral part of the structure but may be a temperature sensor which is insulated from the rest of the structure.

$$\left(\frac{Q}{A}\right)_{\text{aerodynamic}} - \left(\frac{Q}{A}\right)_{\text{radiation}} = \frac{W_1 C_{\cdot}}{A} \dot{T}_1 \tag{13}$$

throughout the trajectory. When the indicated substitutions and grouping of the coefficients are made, the governing differential equation becomes

$$\dot{T}_1 + \xi_1 T_1^4 = \xi_1 T_2^4 + \xi_2 M^{3.1} p^{0.5} \tag{14}$$

where

$$\xi_1 = \frac{k\sigma A}{CW_1} = 0.6 \times 10^{-12}$$

$$\xi_2 = \frac{0.01A}{CW_1 (r^*)^{0.5}} = 0.004417$$

Unless indicated otherwise, equation (14) was used with these values of ξ_1 and ξ_2.

At each position on the trajectory the pressure and Mach number were calculated from the altitude and velocity data from the expressions

$$p = R\rho(h)T(h) \tag{15}$$

$$M = \frac{V}{c} = \frac{V}{\sqrt{\gamma_1 RT(h)}} \tag{16}$$

where γ_1 and R were treated as constants having the values

$$R = 1716.6 \text{ ft}^2/\text{sec-}^\circ\text{R}$$

$$\gamma_1 = 1.4$$

The variables ρ and V were taken directly from the trajectory data, whereas the free-stream temperature T was computed by using straight-line segments to approximate the altitude-temperature plots of reference 6.

At 350,000 feet (h_o for most of the trajectory studies) the equilibrium surface temperature calculated by equation (14) exceeds 1,000° R and the assumption that $\dot{T}_1$ is zero at that condition is not justified. Therefore, trajectories which include temperature calculations were initiated at 550,000 feet where aerodynamic heating is negligible, $\dot{T}_1 \approx 0$, and the surface temperature of the vehicle and the radiation equilibrium temperature are about equal (580° R). Since the angle of attack has virtually no effect on the trajectory above 350,000 feet, only a few cases were calculated at 550,000 feet to establish the value of T_1 and $\dot{T}_1$ at 350,000 feet for each initial condition needed.

TRAJECTORY STUDIES

In order to provide insight into means of regulating the maximum deceleration during the entry, the conditions governing the maximum deceleration are derived. The necessary condition that the deceleration, given by equation (8), be constant or at least an instantaneous maximum is imposed by setting its time derivative equal to zero. Thus for these extremum, the condition

$$\dot{a}_n = \frac{C_F \rho_e e^{-h/H}}{2W/S}\left(-\frac{\dot{h}}{H}V^2 + 2V\dot{V}\right) = 0$$

leads to a necessary condition between the rate of descent and the time rate of change of velocity; that is,

$$\frac{\dot{V}}{g} = \frac{V\dot{h}}{2gH} \tag{17}$$

Expressions for these two derivatives everywhere on the trajectory are given by equation (7). Substituting these expressions into equation (17) and rearranging the terms yield the desired expression for the maximum value of the deceleration

$$(a_n)_{max} = -\frac{\sin\gamma}{\sin\alpha}\left(\frac{V^2}{2gH} + 1\right) \tag{18}$$

For the trajectories controlled with aerodynamic lift, equation (18) shows that the maximum value (or some desired constant value) of deceleration depends directly on the instantaneous values of velocity, angle of attack, and flight-path angle (or rate of descent since $\dot{h} = V \sin \gamma$). As long as the angle of attack is near 90°, its variation at the instant of consideration has very little effect on the magnitude of the deceleration. However, if the angle of attack is used to produce a force normal to the flight path for a sufficient time prior to the time of the maximum deceleration, the magnitudes of both flight-path angle and velocity at the time of maximum deceleration can be reduced to some degree. Likewise if this same force is controlled with the angle of attack throughout the entire atmospheric portion of the entry, it may be aerodynamically possible to hold the deceleration, heating, and range to within some prescribed limits. The angle-of-attack requirements and some methods of application for the aerodynamic control of entry vehicles are investigated in the following sections.

The trajectory results are obtained for a vehicle having an assumed value of the ratio of wing loading to force coefficient $W/C_F S$; however, it is shown in reference 2 (and in appendixes A and C of this paper) that, with an exponential altitude-density relationship, the results are applicable to any value of $W/C_F S$ if the altitude corresponding to each point on the trajectory is shifted by an amount proportional to the logarithm of $W/C_F S$.

Constant-Deceleration Trajectories

The equations of motion given previously may be used to solve for the variation of angle of attack and the resulting variations of altitude and velocity necessary to maintain a constant deceleration during a portion of an entry into the earth's atmosphere. The entry trajectory starts from a zero-g condition and the deceleration increases as aerodynamic drag is encountered. During the final stages of the entry, the deceleration again may decrease as the dynamic pressure falls to values too low to sustain a prescribed value of deceleration. The portion of the trajectory involving constant deceleration is therefore accompanied by transition periods of lower deceleration at the start and finish of the entry. The constant-deceleration period is of interest, however, because a constant-deceleration trajectory will allow the shortest path through the atmosphere without exceeding deceleration values imposed by structural or human physical limits. Furthermore, the oscillations or skipping motions which accompany some constant L/D trajectories (see ref. 2) are eliminated. The results may also prove to be useful as an ideal guide for other types of control.

Since the maximum deceleration occurs at all times colinear with the resultant force, the calculation is restricted to the aerodynamic force and, hence, to the deceleration a_n or $-a_z$. In order to maintain a constant value of deceleration for a given vehicle, the dynamic pressure must remain constant at its corresponding value and, when the exponential approximation to the atmospheric density is used, the relationship between altitude and velocity is fixed. When equation (8) is rearranged, this relationship becomes

$$h = H \log_e \frac{C_F \rho_e}{2W/S} \frac{V^2}{a_n} \tag{19}$$

A plot of the variation of h with V for various values of a_n is shown as figure 2 for a vehicle with a wing loading of 20. It may be seen that from the initial high-velocity high-altitude condition a large reduction in velocity would occur with only a small reduction in altitude. At velocities below 5,000 feet per second a large reduction in altitude would occur with relatively small changes in velocity.

In order to illustrate some of the differences between two types of trajectories, data from a typical high-drag nonlifting ($\alpha = 90^\circ$) entry trajectory are superimposed on the lines of constant deceleration in figure 2. For the zero lift case the flight-path angle is -3° at 350,000 feet and time is indicated on the figure by using dots at 10-second intervals. The vehicle enters the atmosphere at a velocity which has changed very little by the time the deceleration reaches 1 g. Thereafter, the vehicle follows a high deceleration path which dissipates most of the energy over a relatively small range of altitudes.

The initial portion of the nonlifting trajectory is of particular interest. Above 320,000 feet the dynamic pressure is less than 1 pound per square foot. If the descent is not checked, a 3g deceleration is reached at 230,000 feet, 5g at 220,000 feet, and so on. This means that, during the time required to descend 80,000 to 100,000 feet, control of the trajectory by means of the aerodynamic force is available and necessary if the vehicle is to be guided toward an asymptotic intersection with a constant 3g to 5g deceleration trajectory.

The conditions necessary for a vehicle to remain on a constant-deceleration trajectory are investigated next. Development of a form of the basic equations suitable for calculating constant-deceleration trajectories is given in appendix A. The equations were used to compute the trajectories and the variations in angle of attack necessary to achieve

the trajectories for the cases of a_n = 1g, 2g, 3g, and 4g. The computations were performed on a digital computer with a triangular (two-point) integration process.[3] Each trajectory was started at the flight conditions V, γ, h which satisfied the equations when α was exactly 90°, that is, the maximum drag condition. (See eqs. (A16) and (A17).)

Time histories of the trajectories are presented in figure 3. It is noted that the initial value of $\dot{h}$ is almost linearly dependent on the magnitude of the deceleration. From its initial value of 90° the angle of attack decreases; this decrease in angle of attack increases the lift, prevents a rapid increase in flight-path angle or rate of descent, and thus maintains a constant deceleration. As the velocity decreases, however, the requirement (eq. (19)) for lower altitudes leads to ever-increasing rates of descent and flight-path angles. Except in the 1 g case, this demand for higher rates of descent eventually leads to angles of attack greater than 90° and, hence, a negative lift is required to push the vehicle down into the denser atmosphere if a constant deceleration is to be maintained.

The time histories were discontinued at velocities less than 4,000 feet per second. It may be expected, however, that α and $-\gamma$ continue to increase and the velocity continues to decrease until the desired value of deceleration can no longer be obtained. The exception is the 1 g trajectory which the equations indicate can be maintained to sea level where the terminal velocity is about 100 feet per second for α = 90° and W/S = 20. Since the assumed aerodynamic characteristics become inaccurate at low angles of attack as well as at low velocities, the data given for the 1 g trajectory should be viewed as approximate.

From the trajectory data of figure 3, the variation of angle of attack and flight-path angle with velocity is crossplotted in figure 4 to eliminate time as the independent parameter. The results, presented in this form, are very general since wing loading, time, altitude, and force coefficient are not involved in these data as may be seen from the equations of appendix A. The effect of the aforementioned parameters is contained entirely in the altitude-velocity relationship given by equation (19). Therefore, if W/S or C_F are changed, the variables γ, α, $\dot{h}$, $\dot{V}$, and all of their time derivatives remain unchanged as functions of velocity but each velocity on the trajectory occurs at a different time and altitude.

---

[3]By the use of certain approximations, analytical solutions which are valid for a large part of each trajectory may be obtained. These closed-form solutions and the corresponding assumptions are given in the latter part of appendix A and in appendix C.

Control of Angle of Attack As a Function of Deceleration

In order to reduce the peak deceleration from the value obtained with a nonlifting entry trajectory, the control of angle of attack as a linear function of some trajectory variables was tried. One obvious quantity to use for this purpose is the deceleration measured along the Z body axis of the vehicle. Since the resultant aerodynamic force in Newtonian flow is also along this axis, no resolution of accelerations is necessary. For this type of control

$$\alpha = \alpha_o - K_1 a_n \tag{20}$$

and a no-lag response in α to a measured value of a_n is assumed. This would be an ideal choice if, by adjusting K_1, the deceleration could be made to reach some predetermined maximum value and remain in close proximity to that value until the low-speed (that is, under 5,000 feet per second) condition is reached. The constant-deceleration data of figure 4 could then be used as a guide in the choice of K_1.

In order to illustrate these points, the time history of an entry trajectory with the angle of attack held constant at 90° is presented in figure 5(a) and an entry with $\alpha = 90^\circ - 3a_n$ is shown in figure 5(b). The trajectory equations are equations (7), (8), and (9) and the initial conditions in both cases are

$$\alpha_o = 90^\circ$$

$$\gamma_o = -1^\circ$$

$$h_o = 350{,}000 \text{ ft}$$

$$V_o = 25{,}863 \text{ ft/sec}$$

When the angle of attack is held constant at 90° (fig. 5(a)), the deceleration rapidly builds up to a peak value of 8g. With the angle of attack varied according to equation (20), figure 5(b) shows that the rate of descent is reduced and the maximum deceleration is less than 4g.

In the constant-deceleration data of figure 4 the minimum angle of attack for a constant 3g entry is 78° and this occurs at a velocity near 11,000 feet per second. A gain $K_1 = 4$ in equation (20) would likewise produce an angle of attack of 78° whenever $a_n = 3g$. Therefore, the

relative effect of increasing the gain to 4 is illustrated in figure 6. Time histories of deceleration and angle of attack are compared in figure 6 for values of K_1 of 0, 3, and 4. It may be seen that the deceleration was held in the vicinity of 3g when the gain was 4 although some overshoot did occur. The velocity of 11,000 feet per second occurred at 365 seconds for the $K_1 = 4$ case and occurred at 345 seconds for the $K_1 = 3$ case.

In figure 6 and in most ensuing figures, the range Δs is given for each trajectory. The range is defined as the distance in miles traveled over the surface of the earth (nonrotating) from the initial position in space to a point on the trajectory where the range is increasing at less than 100 feet per second. At this condition total velocity is under 5,000 feet per second and the flight path is very nearly vertical ($\gamma \rightarrow -90^\circ$). Since for all trajectories the variations of Δs, V, h, and γ are nearly identical to those given in figure 5, they are not included in the figures.

Figure 7 shows the effect of initial flight-path angle on the deceleration and rate of descent when the angle of attack is controlled according to equation (20). When the initial flight-path angle is between 0° and -1°, the deceleration reaches about the same maximum value. However, at entry angles greater than 1°, the increased rate of descent produces a more rapid increase in deceleration and the consequential reduction in angle of attack does not have time to reduce the flight-path angle and rate of descent sufficiently before large decelerations have been reached. Thus it may be seen from figure 7 that this type of controller, which may be efficient at some specified entry angle, does not possess the ability to anticipate the more rapid changes in deceleration which occur at larger entry angles or higher rates of descent. The key here, then, is anticipation. Several means of obtaining the necessary anticipation are available such as measurements of γ, $\dot{h}$, $\dot{a}_n$, and T_1. If it is known during the early stages of the entry that γ is large, the angle of attack can be reduced to some value less than 90° before the deceleration starts to build up. (This change presumably would require reaction controls.) The same thing could be done by measuring $\dot{h}$ in the early stages of the entry. Further consideration will be given to these and temperature as methods of control in subsequent sections of the paper.

The third method of anticipation, that of $\dot{a}_n$, can be easily added to the present study. The angle of attack and, hence, the lift and flight path may be changed earlier in the entry by making

$$\alpha = \alpha_o - K_1 a_n - K_2 \dot{a}_n \qquad (21)$$

and by properly choosing K_2. As in previous cases, a perfect response in angle of attack to the controls is assumed.

The complete trajectory of a vehicle with this type of angle-of-attack control is shown in figure 8 for an initial flight-path angle of -1°. Gains were set at $K_1 = 3$ deg/g, and $K_2 = 250$ deg/g/sec based on measurements of a_n and $\dot{a}_n$ in the preceding cases. In figure 9 the relative effect of this type of control is compared with the a_n control and the constant 90° angle-of-attack entry of figure 5. The effect of the anticipation term in the angle-of-attack control is to reduce notably the magnitude of the first peak in the deceleration while the magnitude of the second peak remains virtually the same.

A range of values for K_2 is illustrated in figure 10. With the initial conditions of $\alpha_o = 90^\circ$, $\gamma_o = -1^\circ$, and $K_1 = 3$ common to all three cases, the variation of deceleration (to an enlarged scale) and angle of attack with time is shown for the cases of $K_2 = 150$, 250, and 350. The figure illustrates that increasing the value of K_2 primarily suppresses the rate of increase in the deceleration.

Larger values of the initial flight-path angle present a more severe test of the angle-of-attack controller and trajectory data at several entry angles are presented in figure 11. Gains of $K_1 = 4$ and $K_2 = 250$ and an $\alpha_o = 90^\circ$ are used in the angle-of-attack control while entry is initiated at flight-path angles of -1°, -2°, and -3°. The deceleration, rate of change of altitude, and angle of attack of figure 11 may be compared with those of figure 7 [4] where no anticipation was used. With anticipation the deceleration was held within the values of 3.4g to 2.1g. In order to obtain these lower values of decelerations over the range of entry angles, it is necessary to make relatively large changes in angle of attack but at a relatively low rate. For example, when $\gamma_o = -3^\circ$ the minimum angle of attack is 59° but the maximum rate of change of angle of attack required is 1° per second. These values compare with the minimum angle of attack of 67.2° and a maximum rate of 0.52° per second obtained in the $\gamma_o = -3^\circ$ case of figure 7.

The effect of relatively large changes in angle of attack on the deceleration, heating rates, and the temperature of the vehicle is shown in figure 12. In this figure a third possible control function is used,

---

[4] The angle of attack, although not shown, is easily computed from figure 7 since $\alpha = 90^\circ - 4a_z$. At the maximum decelerations, angles of attack of 77.2°, 73.8°, and 67.2° are obtained for the respective entry angles of -1°, -2°, and -3°.

namely, the case where K_1 is set to 0 and $\alpha = 90^\circ - 250\dot{a}_n$. Trajectories using this control function are compared with trajectories when $\alpha = 90^\circ$ on the basis of deceleration, angle of attack, aerodynamic heating rate to the vehicle, and skin temperature for initial flight-path angles of -1°, -2°, and -3°. When compared with the data of the preceding figure (fig. 11), the effect of changing K_1 from 4 to 0 is to increase at all three entry angles the value of the second peak in the deceleration by about 1.5g. From a comparison of the $\alpha = 90^\circ - 250\dot{a}_n$ trajectories with the $\alpha = 90^\circ$ trajectories, the following conclusions are drawn. When the angle of attack is changed in proportion to $\dot{a}_n$, the time histories of deceleration are very similar and have almost the same maximum value for entry angles up through 3°. Heating rates and maximum skin temperatures are virtually unaffected by large reductions in angle of attack from 90° compared with the value obtained when the angle of attack is held constant at 90°. Note that the skin temperature and heating rate reach their maximum values before the deceleration reaches a maximum (exception: a submaximum in the $\gamma_o = -3^\circ$ case); thus, it appears that a reduction in angle of attack to values less than 90° during the initial phase of the trajectory produces as its principal effect a less rapid decrease in the heating rate and temperature during the final phase of the trajectory. This effect results in a slightly larger total heat which must be absorbed by the vehicle but this increase occurs at temperatures less than the maximum.

In all the preceding trajectories it has been assumed that the vehicle was at an angle of attack of 90° when entry was initiated (that is, by the time the vehicle reached 350,000 feet). In figure 13, with an entry angle of -1°, the entry is initiated at angles of attack of 70° and 110° with the $\alpha_o = 90^\circ$ case reproduced for comparison. The type of control assumed for this study is one in which

$$\alpha = \alpha_o - K_1 a_n - K_2 \dot{a}_n$$

where now

$$K_1 = \frac{\alpha_o - \alpha_d}{a_{n,d}}$$

In the expression for K_1, $a_{n,d}$ is the "design deceleration" taken as 3g and α_d is the corresponding minimum angle of attack (78°) for a 3g deceleration as obtained from figure 4. Thus with this control law the angle of attack varies from the value α_o at the start of the entry

(where the deceleration is zero) to the value of α_d when the deceleration reaches design value $a_{n,d}$. When α_o is greater than α_d, K_1 is positive and, as shown in previous figures, a positive K_1 produces a stable variation of angle of attack with deceleration for entry trajectories. When α_o is less than α_d, K_1 is negative, a condition which has not been investigated previously.

For the purposes of computation, the values of K_1 were rounded off to the nearest integer; thus,

$\alpha_o = 110^o$	$K_1 = 10$
$\alpha_o = 90^o$	$K_1 = 4$
$\alpha_o = 70^o$	$K_1 = -3$

As shown in figure 13, the control was effective even when K_1 is negative. The effects of changing density together with the stabilizing contribution of the $\dot{a}_n$ term in the controller act to nullify any rapid increase in angle of attack which would in turn increase the deceleration beyond the desired limits. When this type of controller is used, the differences in range due to the initial difference in angle of attack are very pronounced: With reference to the $\alpha_o = 90^o$ case the range is decreased by about 250 miles when $\alpha_o = 110^o$ and increased by about 900 miles when $\alpha_o = 70^o$.

Trajectories for Vehicles Trimmed at Angles of Attack Less Than 90°

In the preceding sections it has been shown that the deceleration during reentry may be limited to small oscillations about some mean value when the angle of attack is reduced from 90° to some lesser value as a function of a_n and $\dot{a}_n$. When the angle of entry was greater than 1°, however, large changes in angle of attack were necessary to prevent large overshoots in deceleration. By entering the atmosphere at angles of attack less than 90°, it may be possible to obtain a compromise between drag and deceleration which would allow smaller and even less rapid changes in angle of attack and still retain a high ratio of wave drag to viscous drag in order to minimize heating of the vehicle. In figure 14 trajectory data for four entry angles are shown for the condition where

the angle of attack is held constant at 79°. For entry angles up to 2° the deceleration was limited to 3.3g while at a 3° entry the deceleration reached 4.8g. However, these values represent an appreciable reduction in deceleration over the 8g to 11g range when the angle of attack is held constant at 90° during the entry. (See fig. 12.)

A comparison of the aerodynamic heat-transfer rates and vehicle skin temperatures is shown in figure 15 for the $\alpha = 90°$ and $\alpha = 79°$ cases and for entry angles of 1° and 3°. When the entry angle was 1°, the vehicle maintained at $\alpha = 79°$ had a lower aerodynamic heat-transfer rate and a maximum skin ($W_1C/A = 0.8$) temperature that was lower by 100° R than that for the vehicle maintained at $\alpha = 90°$. Total heat transferred to the vehicle through aerodynamic heating, as measured by the time integral of the aerodynamic heating rate, appears to be one-third greater when the angle of attack is held at 79°.

The $\gamma_o = -2°$ case is not shown in figure 15 since it afforded no additional information. When $\gamma_o = -3°$ the maximum values of aerodynamic heat-transfer rate and skin temperature are about the same at either angle of attack. For both entry angles shown, the total heat transferred is considerably increased when $\alpha = 79°$ as compared with the $\alpha = 90°$ case. The increase in heat transfer may be further compared with the cases shown in figure 12. In figure 12 the angle of attack was increased to angles greater than 90° as soon as the deceleration had been checked, rather than holding it constant at 79° throughout the trajectory as was done in figure 15. It may be seen that the type of angle-of-attack control used in figure 12 results in a total heat transfer which is much lower than that obtained in figure 15 when α is held constant at 79°. This difference in total heat transfer may be important for vehicles which depend to some degree upon ablation materials for heat protection.

A comparison between entries made at a constant angle of attack (other than 90°) and entries made with the angle of attack varied (from its initial value) as a function of $\dot{a}_n$ is shown with two examples in figure 16. In figure 16(a) the time histories of a_n and α are shown for an initial flight-path angle of 3° and with $\alpha = 79° - 100\dot{a}_n$. The effect of the anticipation is to reduce the maximum value of a_n by about 1.2g with an 11° variation in α and to increase the range by 104 miles. The rate of change of angle of attack did not exceed 0.5° per second.

In figure 16(b) trajectory data are shown for the same conditions as figure 16(a) except that α_o is 84°. When the angle of attack is held at 84°, the deceleration reaches 6.8g. When α is changed in

proportion to $\dot{a}_n$, a 12° variation in α is sufficient to reduce the deceleration by 2.4g while the range is increased by 110 miles.

From a number of such trajectories a summary plot of range and maximum deceleration as a function of entry angle is presented in figure 17. It was assumed in obtaining these data that 79° was the desired angle of attack but that a ±5° error in α_o might occur. Therefore, the data are given for initial values of α of 84°, 79°, and 74° for cases where the $\dot{a}_n$ gain is 0 and 100. The data show that, when the $\dot{a}_n$ control is included, the deceleration is reduced, particularly at the higher entry angles, while the range is extended by less than 110 miles.

Within the conditions investigated, the data of figure 17 indicated that

$$\text{Range} \propto \gamma_o^{-0.58}$$

when the anticipation control is included. The range does not exactly follow a power relationship, however, when the angle of attack is held constant.

Trajectories Made at a Constant Rate of Descent

In several places in the preceding sections it has been pointed out qualitatively that rate of descent and maximum deceleration are closely related during the atmospheric entry. Allen and Eggers (ref. 1) have shown that, for a nonlifting body passing through the atmosphere at a large constant flight-path angle ($\gamma(t) = \gamma_o$, force of gravity being neglected), the maximum deceleration obtained is directly proportional to the velocity and rate of descent. This proportionality can be shown to be more general than the limitations imply. For all trajectories, including those initiated at small flight-path angles, the condition of maximum deceleration was derived as equation (18). When $V \sin \gamma$ is replaced with $\dot{h}$, equation (18) can be arranged in the form:

$$(a_n)_{max} = \frac{-\dot{h}V}{2gH \sin \alpha}\left(1 + \frac{2gH}{V^2}\right)$$

$$(a_n)_{max} \approx \frac{-\dot{h}V}{2gH}$$

The approximate expression is comparable to that given (with some difference in symbols) in reference 1 and the limitations may be seen to be that $\alpha = 90^{\circ}$ since for high-drag low-lift vehicles, in general, $\frac{2gH}{V^2} < 0.01$ when the maximum deceleration occurs.

A special case of interest is the trajectory where the pilot maintains a constant rate of descent during the entry. It is presumed that the vehicle is initially at an angle of attack of 90° at 350,000 feet and has a velocity of 25,863 feet per second. The condition of constant rate of descent is imposed. Since velocity is specified, the initial flight-path angle determines an initial magnitude of $\dot{h}$ and the angle of attack is then varied such as to maintain the condition $\dot{h}(t) = \dot{h}_o$ as long as it is aerodynamically practical.

The development of the equations used to calculate this type of entry is given in appendix B.[5] By using these equations, time histories of constant-rate-of-descent trajectories are presented in figure 18 for four different rates of descent determined by the four intial flight-path angles selected.

The data indicate that throughout most of the trajectory only moderate changes in angle of attack are required for this type of entry. It is further shown that maximum deceleration occurs at the same velocity ($\approx$13,100 ft/sec) and about the same altitude ($\approx$178,000 feet) regardless of the rate of descent chosen and that therefore the magnitude of the maximum deceleration is a linear function of rate of descent (or flight-path angle) only.

A summary plot of the variation of range and deceleration with entry angle is shown in figure 19 for the constant $\dot{h}$ trajectories. The linear variation of deceleration with initial flight-path angle is given by

$$(a_n)_{max} = -4\gamma_o$$

where γ_o is in degrees. Range follows a power relationship to initial flight-path angle given by

---

[5]By the use of certain approximations, analytical solutions may be obtained which are valid for a large part of each trajectory. The approximations and the closed-form solutions are given in appendix C.

$$\Delta s \propto \gamma_o^{-0.87}$$

but the significance of this fact is not evident.

Angle of Attack Controlled as a Function of Temperature

Normally, in order to control the deceleration, it would appear to be advantageous to observe deceleration and vary the angle of attack accordingly. It has been shown, however, that because of the time required to change the flight path a certain amount of anticipation should be employed in the control of angle of attack and that $\dot{a}_n$, γ_o, or $\dot{h}_o$ can be used to give this anticipation. A basic trajectory variable which may also contain the information useful to the control of both heating and deceleration is the skin temperature. This variable, unlike $\dot{a}_n$, can be measured directly and in some cases may tend to lead the deceleration and provide the required anticipation. Some of the quantities pertaining to the skin temperature obtained on a vehicle during an entry are illustrated in figure 20.

Shown in figure 20 are the calculated data for a typical time history of an atmospheric entry. The altitude at the start of the time history is 550,000 feet and the conditions at 150 seconds are $h = 350{,}000$ ft, $V = 25{,}863$ ft/sec, $\gamma = -3^\circ$, and $\alpha = 90^\circ$. The angle of attack was held fixed at 90° during the entire trajectory. The quantities shown are: deceleration, a_n; time rate of change of deceleration, $\dot{a}_n$; skin temperature for a unit area of material having a heat-capacity factor of 0.8, T_1, and material having a heat-capacity factor of 0.2, $T_1{}^*$; the free-stream temperature, T; the rate of change of the two skin temperatures, $\dot{T}_1$ and $\dot{T}_1{}^*$; and the heating rate to the skin from the boundary layer, $(Q/A)_{aero}$.

It may be seen that T_1 and a_n have, in general, the same shape and each reaches a maximum at about the same time. Likewise, $\dot{a}_n$ and $\dot{T}_1$ have the same shape, both go negative at the same time although $\dot{T}_1$ leads $\dot{a}_n$ by about 20 seconds in reaching a maximum. The aerodynamic heating rate appears to be strongly influenced by the time rate of

change of density or dynamic pressure[6] since it also reaches a maximum with $\dot{a}_n$.

When the insulated unit area of surface material is changed by using a different material or a different thickness such that its heat capacity is reduced by a factor of 4 (W_1C/A reduced from 0.8 to 0.2), the temperature T_1^* increases more rapidly and reaches a higher maximum value sooner than the material with the higher heat capacity. Therefore, by adjusting the heat capacity, the temperature can be made to lead the deceleration and to reach a maximum at about the same time as $\dot{a}_n$. By using this lead, it was thought that T_1^* might exhibit characteristics similar to $\dot{a}_n$ in the control of angle of attack. Trajectories covering the range-of-entry angles were calculated by using ΔT_1^* (base value was T_1^* at 550,000 feet) to control angle of attack and the results are shown in figure 21. It was found that the trajectories were almost identical to those obtained with the $\alpha \propto a_n$ control of figure 7. At an entry angle of 3° the lead effect held the deceleration to 4g but large oscillations in deceleration still occurred as they did with the a_n control. A further disadvantage in the use of T_1 or T_1^* lies in the practical uncertainty of choosing a gain for a variable which does not start from a firmly established base value. On the other hand, the fact that $\dot{T}_1$ has about the same variation as $\dot{a}_n$ during an entry makes $\dot{T}_1$ appear promising as a variable for controlling angle of attack.

One further combination of variables which appears to offer some promise is the quantity $T_1^* - T_1$. As can be seen from figure 20, the difference $T_1^* - T_1$ is zero at the start of the entry, builds up to a positive maximum before $\dot{a}_n$, and becomes negative at about the same time as $\dot{a}_n$. A study of a number of trajectories shows this to be a general characteristic and that the magnitude of $T_1^* - T_1$ decreases with decreasing entry angles.

---

[6]Dynamic pressure has the same time history as a_n but has the magnitude $q = \frac{W/S}{C_F} a_n$ where $\frac{W/S}{C_F} = \frac{20}{1.7}$ lb/sq ft for all trajectories of this report. Likewise, $\dot{q} = \frac{W/S}{C_F} \dot{a}_n$. By neglecting the variation of T, it can be shown that $(Q/A)_{aero} \propto \dot{q}^{1.55} \rho^{-1.05}$. Thus, the effect of ρ on the heating rate is that of an exponential decrease in amplitude which shifts the peak magnitude of the heat-transfer rate ahead of the peak deceleration in time.

CONCLUDING REMARKS

Numerical computations have been made for the trajectories of high drag vehicles entering the earth's atmosphere at large angles of attack and pertinent data from these computations have been presented. When the trajectories were calculated it was assumed that angle of attack could be perfectly controlled as a function of some measured quantity, held constant at some specified value, or moved (in a continuous manner) to maintain one of the other variables at some constant value. The results represent large-scale motions of a vehicle which is capable of producing lift while descending into the earth's atmosphere from initially small flight-path angles and near-satellite velocities. Newtonian flow was assumed in calculating the aerodynamic force on the vehicle through the trajectory.

The velocity, altitude, flight-path angle, and angle-of-attack requirements necessary to maintain (but not to establish) constant deceleration entries of 1g, 2g, 3g, and 4g were calculated and used as a guide for determining methods of controlling the angle of attack so as to limit the deceleration to the arbitrarily chosen value of 3g. When the angle of attack was changed from 90° in proportion to the deceleration only, it was found that deceleration could be limited to the vicinity of 3g as long as the initial flight-path angle was under 2° but at 3° the control was inadequate and large oscillations occurred about this mean value of deceleration.

When the angle of attack was controlled as a function of a_n and $\dot{a}_n$ from its initial value of 90°, deceleration could be held to a maximum of 3g for all entry angles to 3°. Trajectories where angle of attack was a function of $\dot{a}_n$ only likewise had about the same maximum value of deceleration at all entry angles but the level of this maximum deceleration was larger (about 4.7g) than when angle of attack was a function of both a_n and $\dot{a}_n$.

Range and deceleration data were presented for trajectories where angle of attack was held constant at values of 84°, 79°, and 74° and for trajectories where angle of attack was changed from these values in proportion to $\dot{a}_n$. It was found that, when the entry was initiated at these lower angles of attack and then varied as a function of $\dot{a}_n$, smaller and less rapid changes in angle of attack were necessary to achieve the desired levels of deceleration than were necessary when α_o was 90°.

The angle-of-attack requirements necessary to maintain constant rates of descent throughout the entry were investigated and were found

to be very moderate. In addition, the maximum deceleration is a linear function of that rate of descent only, and the altitude and velocity at which the maximum deceleration occurs are virtually independent of the rate of descent chosen. Thus, for a vehicle of given wing loading, the altitude and velocity at which the deceleration reaches a maximum will always be the same regardless of rate of descent.

By using a simple model of the exposed skin surface of the vehicle, the heating rates and skin temperatures were calculated for a number of these trajectories. It was shown that, when the angle of attack is reduced from 90° to 79° or is varied as a function of $\dot{a}_n$ while the deceleration is controlled, the maximum rate of aerodynamic heat transfer to the skin is reduced, the maximum skin temperature of the vehicle is virtually unaffected, and the total heat to the vehicle is slightly increased. The increases in total heat transfer can be minimized by holding the maximum desired deceleration for as much of this trajectory as possible since total heat increases with the total time to enter.

The feasibility of using a small insulated section of the skin for temperature measurements and the use of the measured temperatures for angle-of-attack control was investigated. Skin temperature had the same time-history characteristics as deceleration, and the time rates of change of these two variables were likewise very similar throughout the trajectory. Temperatures could be made to lead the deceleration by reducing the heat capacity of the material. With and without this lead, the use of temperature to control angle of attack produced trajectories very similar to those obtained when angle of attack was controlled by deceleration. A simple means of anticipating the increase in deceleration and heating rates is to measure the difference in temperature between two adjacent sections of the skin of the vehicle having different levels of conductivity.

Langley Research Center,
National Aeronautics and Space Administration,
Langley Field, Va., October 13, 1958.

APPENDIX A

EQUATIONS FOR CONSTANT DECELERATION TRAJECTORIES

The basic differential equations for an entry into the earth's atmosphere are

$$\frac{\dot{V}}{g} = -a_n \sin \alpha - \sin \gamma \tag{A1}$$

$$\frac{V}{g} \dot{\gamma} = a_n \cos \alpha + \left(\frac{V^2}{g_r} - 1 \right) \cos \gamma \tag{A2}$$

$$\dot{h} = V \sin \gamma \tag{A3}$$

For constant-deceleration trajectories, it is further required that

$$a_n = -a_z = \frac{C_F \rho_e}{2W/S} e^{-h/H} V^2 = \text{Constant} \tag{A4}$$

The object is to find the variation of angle of attack which will satisfy these equations at every point on the trajectory. The other variables are dependent on the proper choice of α and they are determined in the process.

From equation (A4) the relationship between altitude and velocity for the constant values of deceleration and wing loading is given by

$$h = H \log_e \frac{C_F \rho_e}{2W/S} \frac{V^2}{a_n} \tag{A5}$$

The condition that $\dot{a}_n$ be zero (see eq. (17)) defines a necessary relationship between $\dot{h}$ and $\dot{V}$; namely,

$$V\dot{h} = 2H\dot{V} \tag{A6}$$

A second differentiation gives

$$\ddot{h} = 2H\left[\frac{\ddot{V}}{V} - \left(\frac{\dot{V}}{V} \right)^2 \right] \tag{A7}$$

Thus h and its time derivatives are defined in terms of V and its derivatives.

The flight-path angle may likewise be related to velocity. From equations (A3) and (A6),

$$\gamma = \sin^{-1} \frac{\dot{h}}{V}$$

$$\gamma = \sin^{-1} \frac{2H}{V^2} \dot{V} \tag{A8}$$

Differentiating equation (A8) and making the substitution

$$\cos \gamma = \left[1 - \left(\frac{2H}{V^2} \dot{V} \right)^2 \right]^{1/2} \tag{A9}$$

yield

$$\dot{\gamma} = \frac{2H}{V \cos \gamma} \left[\frac{\ddot{V}}{V} - 2 \left(\frac{\dot{V}}{V} \right)^2 \right] \tag{A10}$$

The time rate of change of velocity is derived from equations (A1) and (A8) in terms of angle of attack and velocity as

$$\dot{V} = \frac{-ga_n \sin \alpha}{1 + \frac{2gH}{V^2}} \tag{A11}$$

Differentiation of equation (A11) with respect to time and elimination of $\dot{V}$ give an expression for the second derivative of velocity

$$\ddot{V} = \frac{g}{H} \left(\frac{V \sin^2 \gamma - Ha_n \cos \alpha \dot{\alpha}}{1 + \frac{2gH}{V^2}} \right) \tag{A12}$$

Equations (A2), (A8), (A10), (A11), and (A12) together with an equation for $\dot{\alpha}$ represent six equations with six unknowns at each value of time. The equation for $\dot{\alpha}$ is unspecified but one may be manufactured in several ways, the most convenient being

$$\dot{\alpha} = \frac{\Delta \alpha}{\Delta V} \dot{V} \tag{A13}$$

Thus for a given change in velocity, equations (A11) and (A13) depend only on the corresponding change in angle of attack. The integration

process enters the equations only through calculation of the $\dot{\alpha}$ term, a variable which is generally small. Since a constant-deceleration entry is being considered, $\dot{V}$ should be very nearly constant over each Δ interval of integration. In the calculations of this paper, for each small reduction in velocity from V_n to V_{n-1}, equation (A13) was applied in the form

$$\dot{\alpha}_n = \frac{\alpha_n - \alpha_{n-1}}{V_n - V_{n-1}} \frac{1}{2(57.3)} \left(\dot{V}_n + \dot{V}_{n-1} \right) \tag{A14}$$

to determine the nth value of $\dot{\alpha}$. The corresponding value of time is given by

$$t_n = t_{n-1} + \frac{V_n - V_{n-1}}{\frac{1}{2}\left(V_n + \dot{V}_{n-1} \right)} \tag{A15}$$

It is useful in determining the initial velocity to combine equations (A2), (A8), (A10), (A11), and (A12) into the following equations:

$$\frac{2 \sin \alpha \tan \gamma}{\left(1 + \frac{2gH}{V^2} \right)^2} + \left(1 - \frac{V^2}{gr} \right) \frac{\cos \gamma}{a_n} = \cos \alpha - \frac{V}{a_n g} \frac{\tan \gamma}{\tan \alpha} \dot{\alpha} \tag{A16}$$

$$\sin \gamma = \frac{-2gHa_n \sin \alpha}{V^2 + 2gH} \tag{A17}$$

Thus, when a_n, α, and $\dot{\alpha}$ are specified, these two equations determine the corresponding value of the velocity.

For a given deceleration the maximum entry angle is obtained when α is 90°, as may be seen from equation (A17). Since the terms involving $\dot{\alpha}$ in equations (A12) and (A16) become zero when α is 90°, this condition affords an initial condition where all the variables are known. Thereafter, a ΔV interval is chosen, a value of α is assumed at the new velocity, and equations (A11), (A14), (A12), (A8), (A10), and (A2) are solved in that order to yield a new value of α. An iteration process is used until the assumed and derived values of α are in agreement. The iteration process is easily handled on a high-speed digital computer and at the higher values of velocity the process is highly convergent.

A very good approximate closed-form solution is available based on the assumption that

$$\sin \alpha = \text{Constant} = 1.0$$

With this assumption, equation (A11) may be integrated to give the velocity as a function of time

$$V(t) = \sqrt{\beta(t)^2 + 2gH} - \beta(t) \tag{A18}$$

where

$$\beta(t) = \frac{1}{2} a_n g t - V_o + \frac{2gH}{V_o}$$

When V is given as a function of the time and $\sin \alpha$ is treated as a constant with a value of unity, the other variables may be directly calculated as follows:

$$\left.\begin{aligned}
\dot{V} &= \frac{-g a_n}{1 + \frac{2gH}{V^2}} \\
\ddot{V} &= \frac{g}{H} \frac{V \sin^2 \gamma}{1 + \frac{2gH}{V^2}} \\
\gamma &= \sin^{-1} \frac{-2gHa_n}{V^2 + 2gH} \\
\dot{\gamma} &= \frac{2H}{V \cos \gamma}\left[\frac{\ddot{V}}{V} - 2\left(\frac{\dot{V}}{V}\right)^2\right] \\
h &= H \log_e \frac{C_F \rho_e}{2W/S} \frac{V^2}{a_n} \\
\dot{h} &= 2H \frac{\dot{V}}{V}
\end{aligned}\right\} \tag{A19}$$

Making the indicated substitutions in equation (A2) or applying the assumption to equation (A16) then yields an expression for $\alpha(t)$

$$\cos \alpha = \frac{2 \tan \gamma}{\left(1 + \frac{2gH}{V^2}\right)^2} + \left(1 - \frac{V^2}{gr}\right)\frac{\cos \gamma}{a_n} \tag{A20}$$

This approximate solution leads to results very close to those obtained by the iterative integral method as long as α remains near 90°. However, the solution becomes imaginary when the quantity

$$\frac{2gHa_n}{V^2 + 2gH} > 1$$

At this velocity no real value of γ exists which will satisfy the equations.

APPENDIX B

EQUATIONS FOR CONSTANT RATE OF DESCENT TRAJECTORIES

The basic equations for trajectories into the earth's atmosphere where rate of descent is maintained at some constant value are given by

$$\frac{\dot{V}}{g} = -a_n \sin \alpha - \sin \gamma \tag{B1}$$

$$\frac{V\dot{\gamma}}{g} = a_n \cos \alpha + \left(\frac{V^2}{gr} - 1\right)\cos \gamma \tag{B2}$$

$$\dot{h} = \dot{h}_o = V \sin \gamma \tag{B3}$$

$$a_n = \frac{C_F \rho_e}{2W/S} e^{-h/H} V^2 \tag{B4}$$

From equation (B3), the following variables are extracted:

$$\dot{h} = \dot{h}_o \tag{B5}$$

$$h = \dot{h}_o t + h_o \tag{B6}$$

$$\gamma = \sin^{-1} \frac{\dot{h}_o}{V} \tag{B7}$$

$$\dot{\gamma} = \frac{-\dot{V} \tan \gamma}{V} \tag{B8}$$

Equation (B8) expresses the required relationship between $\dot{\gamma}$ and $\dot{V}$ necessary to maintain a constant rate of descent and relates equation (B1) to equation (B2). By substituting equation (B8) into equation (B2) to eliminate $\dot{\gamma}$ and then using equation (B1) to eliminate $\dot{V}$, the following relationship between γ and α is obtained:

$$a_n \cos(\alpha + \gamma) = 1 - \frac{V^2}{gr} \cos^2 \gamma \tag{B9}$$

Therefore if $\dot{V}$ and $\dot{\gamma}$ are to be related properly, then α must follow the relationship

$$\alpha = -\gamma + \cos^{-1}\left[\frac{1}{a_n}\left(1 - \frac{V^2}{gr}\cos^2\gamma\right)\right] \tag{B10}$$

If the initial values of h, V, and γ (or $\dot{h}$), are specified, the other variables may be calculated at these initial conditions. An integration process is used to establish approximate values of V and γ at the end of the given time interval. Equations (B6), (B4), (B10), (B1), and (B8) are solved in that order and a new approximation to V and γ made. The process may be repeated but convergence is generally rapid. From the calculated values of V and γ, equation (B3) is solved for $\dot{h}$ at that point on the trajectory. Any inaccuracy in the integration process will produce an $\dot{h}$ different from its initial value and this error is carried over to the next point on the trajectory. Thus, the values of $\dot{h}$ calculated at each point along the trajectory depend directly upon the cumulative accuracy of the integration process and serve as a measure of that accuracy. The effect of these errors shows up in figure 18 as a slight departure of the rate of descent from its initial value. In all cases this error was less than 3.5 percent at the end of the calculations.

APPENDIX C

APPROXIMATE ANALYTICAL SOLUTIONS TO CONSTANT-DECELERATION AND CONSTANT-RATE-OF-DESCENT TRAJECTORIES

It has been pointed out that, by using the "Z" function derived by Chapman (ref. 2), certain closed-form solutions can be made for the trajectories of constant deceleration and constant rate of descent. Solutions can also be obtained directly from the basic equations of this paper by applying the approximations used in reference 2, and this method is used here. In so doing, it is felt that a better physical understanding of the origin and limitations of each solution can be retained.

For most of these closed-form solutions, it is necessary to make the following assumptions:

(a) $|\gamma|$ is small; thus, $\cos\gamma = 1$ and $\tan\gamma = \sin\gamma$

(b) $\left|\frac{\pi}{2} - \alpha\right|$ is small; thus, $\sin\alpha = 1$ and $\cot\alpha = \cos\alpha$

(c) $\frac{V^2}{2gH} >>> 1$

(d) $-\frac{\dot{V}}{g} \approx a_n$

Although these assumptions may appear to be rather restrictive, they are generally valid on that portion of the trajectory of the most interest, namely, the region of maximum heating and deceleration. It may be seen from equation (A1) that assumption (d) is violated at the beginning of the entry when $a_n \approx -\gamma$ but the effect is not serious since $\dot{V}/g$ is small at this point. At the later stages of the entry all the assumptions are generally invalid.

Chapman's symbol for the ratio of velocity along the trajectory to the initial circular satellite velocity

$$\bar{u} \equiv \frac{V}{\sqrt{gr}}$$

is used in this appendix. Thus, for entries from circular and near-circular orbits, $\bar{u}_o$ can be set to unity.

Constant-Deceleration Trajectories

Closed-form solutions for constant-deceleration trajectories based only on the assumption that $\sin \alpha = 1$ are given in the latter part of appendix A. Further simplifications, based on the foregoing assumptions, lead to the analytical solutions which follow.

In view of the assumptions, the normal acceleration a_n, its component in the direction of the velocity $a_n \sin \alpha$, and its horizontal component $a_n \sin \alpha \cos \gamma$ are all approximately the same. For a specified constant value of a_n, equation (A19) gives the expression for the flight-path angle

$$\sin \gamma \approx \frac{-a_n}{\frac{r}{2H}\bar{u}^2} \approx \frac{-a_n}{450\bar{u}^2} \tag{C1}$$

From equation (A20) the angle of attack becomes

$$\left.\begin{aligned} \cos \alpha \approx \frac{L}{D} &\approx \frac{-2a_n}{\frac{r}{2H}\bar{u}^2} + \frac{1 - \bar{u}^2}{a_n} \\ &= \frac{1 - \bar{u}^2}{a_n} - \frac{a_n}{225\bar{u}^2} \end{aligned}\right\} \tag{C2}$$

The incremental change in time from u_{n-1} to u_n is calculated from

$$\Delta t \approx \frac{-\Delta V}{g a_n} = \frac{808}{a_n}\left(\bar{u}_{n-1} - \bar{u}_n\right) \tag{C3}$$

The incremental change in range is given by

$$\left.\begin{aligned} \Delta\left(\frac{\Delta S}{r}\right) &\approx \frac{1}{r}\int_{t_{n-1}}^{t_n} V\, dt \\ &\approx \frac{1}{r\dot{V}}\int_{V_{n-1}}^{V_n} V\, dV \\ &\approx \frac{1}{2a_n}\left(\bar{u}_{n-1} - \bar{u}_n\right) \end{aligned}\right\} \tag{C4}$$

The altitude-velocity relation given by equation (A4) becomes, in terms of $\bar{u}$:

$$h = H \log_e\left(\frac{C_F \rho_e}{2W/S}\, gr\, \frac{\bar{u}^2}{a_n}\right) \tag{C5}$$

When desired, the derivatives of the various variables are given with fewer restrictions by equations (A19).

Constant-Rate-of-Descent Trajectories

From equation (B7) the flight-path angle during the descent is given by

$$\sin \gamma = \frac{V_o \sin \gamma_o}{V}$$

or

$$\sin \gamma = \frac{\bar{u}_o}{\bar{u}} \sin \gamma_o \tag{C6}$$

The deceleration can be obtained in closed form by integrating

$$\dot{h} = V \sin \gamma = V_o \sin \gamma_o \tag{C7}$$

Since

$$\dot{h} = \frac{dh}{dV}\dot{V}$$

and

$$a_n \approx \frac{-\dot{V}}{g}$$

equation (C7) becomes

$$-g a_n\, dh = V_o \sin \gamma_o\, dV$$

Dividing both sides by V^2, substituting for a_n its definition given by equation (B4), and integrating from initial to some arbitrary condition of V, h gives

$$-g\left(\frac{C_F\rho_e}{2W/S}\right)\int_{-h_o}^{h} e^{-h/H}\,dh = V_o \sin\gamma_o \int_{V_o}^{V}\frac{dV}{V^2}$$

$$gH\left[a_n - \left(\frac{V}{V_o}\right)^2 a_{n_o}\right] = -\left(V_o \sin\gamma_o\right)V\left(1 - \frac{V}{V_o}\right)$$

and finally in terms of $\bar{u}$

$$a_n = \frac{-r}{H}\left(\bar{u}_o \sin\gamma_o\right)\bar{u}\left(1 - \frac{\bar{u}}{\bar{u}_o}\right) + \frac{\bar{u}}{\bar{u}_o}\,a_{n_o}$$

$$a_n \approx -900\bar{u}_o \sin\gamma_o\bar{u}\left(1 - \frac{\bar{u}}{\bar{u}_o}\right) \tag{C8}$$

This deceleration is a maximum when

$$\bar{u} = \frac{\bar{u}_o}{2} \tag{C9}$$

and the value of this maximum deceleration is

$$\left(a_n\right)_{max} \approx -225\bar{u}_o\left(\bar{u}_o \sin\gamma_o\right)$$

$$\left(a_n\right)_{max} \approx 3.93\left(-\gamma_o\right) \tag{C10}$$

where γ_o is small and is given in degrees.

Since a_n is defined, the variation in angle of attack is given by writing equation (B9) in the form

$$\cos\alpha\cos\gamma - \sin\alpha\sin\gamma = \frac{1}{a_n}\left(1 - \bar{u}^2\cos^2\gamma\right)$$

By virtue of the assumption that $\cos\gamma = \sin\alpha = 1$, this equation can be approximated with

$$\cos\alpha \approx \frac{L}{D} \approx \sin\gamma + \frac{1}{a_n}\left(1 - \bar{u}^2\right) \tag{C11}$$

or as a function of $\bar{u}$ only

$$\cos \alpha \approx \frac{L}{D} \approx \frac{\bar{u}_o \sin \gamma_o}{\bar{u}} - \frac{1}{900\left(\bar{u}_o \sin \gamma_o\right)\bar{u}} \tag{C12}$$

The altitude h is given by equation (B6) in terms of known initial condition h_o, $\dot{h}_o$ and time. Time is related to $\bar{u}$ by integrating the approximate expression

$$\frac{\dot{V}}{g} \approx -a_n \approx 900\left(\bar{u}_o \sin \gamma_o\right)\bar{u}\left(1 - \frac{\bar{u}}{\bar{u}_o}\right)$$

Thus

$$\int_{t_{n-1}}^{t_n} dt \approx \frac{\sqrt{gr}\ \bar{u}_o}{900g\left(\bar{u}_o \sin \gamma_o\right)} \int_{\bar{u}_{n-1}}^{\bar{u}_n} \frac{d\bar{u}}{\bar{u}\left(\bar{u}_o - \bar{u}\right)}$$

yields

$$\Delta t = t_n - t_{n-1} \approx \frac{0.9}{\bar{u}_o \sin \gamma_o} \log_e \frac{\bar{u}_n\left(\bar{u}_o - \bar{u}_{n-1}\right)}{\bar{u}_{n-1}\left(\bar{u}_o - \bar{u}_n\right)} \tag{C13}$$

The incremental change in range is given by

$$\Delta\left(\frac{\Delta s}{r}\right) \approx \frac{1}{r}\int_{t_{n-1}}^{t_n} V\, dt \approx \int_{\bar{u}_{n-1}}^{\bar{u}_n} \frac{\bar{u}\, d\bar{u}}{-a_n}$$

Substituting equation (C8) for a_n and integrating yield

$$\Delta\left(\frac{\Delta s}{r}\right) \approx \frac{1}{900 \sin \gamma_o} \log_e \frac{\bar{u}_o - \bar{u}_{n-1}}{\bar{u}_o - \bar{u}_n} \tag{C14}$$

Some of the deductions and comments of the text are more clearly indicated by the foregoing approximations. For example, the deductions that, for a constant rate of descent, the velocity at maximum deceleration is independent of entry angle and that the solutions are independent of $W/C_F S$ and density, except for the altitude-velocity relationship, are seen in these solutions.

All the foregoing equations may be derived in the nondimensional form of reference 2.[1] In the notation of reference 2, the horizontal component of deceleration is given therein as

$$a_\theta \approx \frac{\beta r \bar{u} Z}{\cos \varphi} \approx 30 \bar{u} Z$$

where $\beta \equiv \frac{1}{H}$ of this paper, $\bar{u} = \frac{u}{\sqrt{gr}} = \frac{V \cos \gamma}{\sqrt{gr}}$ is the nondimensional horizontal component of velocity, $\varphi \equiv \gamma$ of this paper, and the function Z (in terms of the notation of this paper) is

$$Z \equiv \frac{C_F \rho_e}{2W/S} \sqrt{gH}\, e^{-h/H} V \sin \alpha \cos \gamma$$

$$\equiv \sqrt{gH} \frac{a_n}{V} \sin \alpha \cos \gamma$$

For $\sin \alpha = \cos \gamma = 1$,

$$30 \bar{u} Z \approx a_n$$

which is the reason the results for the constant-deceleration trajectories are the same in either system of coordinates as long as the assumptions are valid.

---

[1]For constant-deceleration trajectories $Z = \frac{a_\theta}{30\bar{u}}$ and for constant-rate-of-descent trajectories $Z = -30\bar{u}_o \sin \varphi_o \left(1 - \frac{\bar{u}}{\bar{u}_o}\right)$.

REFERENCES

1. Allen, H. Julian, and Eggers, Alfred J., Jr.: A Study of the Motion and Aerodynamic Heating of Missiles Entering the Earth's Atmosphere at High Supersonic Speeds. NACA TN 4047, 1957. (Supersedes NACA RM A53D28.)

2. Chapman, Dean R.: An Approximate Analytical Method for Studying Entry Into Planetary Atmospheres. NACA TN 4276, 1958.

3. Ames Research Staff: Equations, Tables, and Charts for Compressible Flow. NACA Rep. 1135, 1953. (Supersedes NACA TN 1428.)

4. Romig, Mary F.: Stagnation Point Heat Transfer for Hypersonic Flow. Jet Propulsion (Technical Notes), vol. 26, no. 12, Dec. 1956, pp. 1098-1101.

5. Hastings, S. M., Persh, J., and Redman, E. J.: Experimental Investigation of the Pressure Distribution on Axi-Symmetric Flat-Face Cone-Type Bodies at Supersonic and Hypersonic Speeds. NAVORD Rep. 5659 (Aerodynamics Res. Rep. 3) U. S. Naval Ord. Lab. (White Oak, Md.), Oct. 1, 1957.

6. Minzner, R. A. and Ripley, W. S.: The ARDC Model Atmosphere, 1956. Air Force Surveys in Geophysics No. 86 (AFCRC TN-56-204) Geophysics Res. Div., AF Cambridge Res. Center (Bedford, Mass.), Dec. 1956. (Available as ASTIA Doc. 110233.)

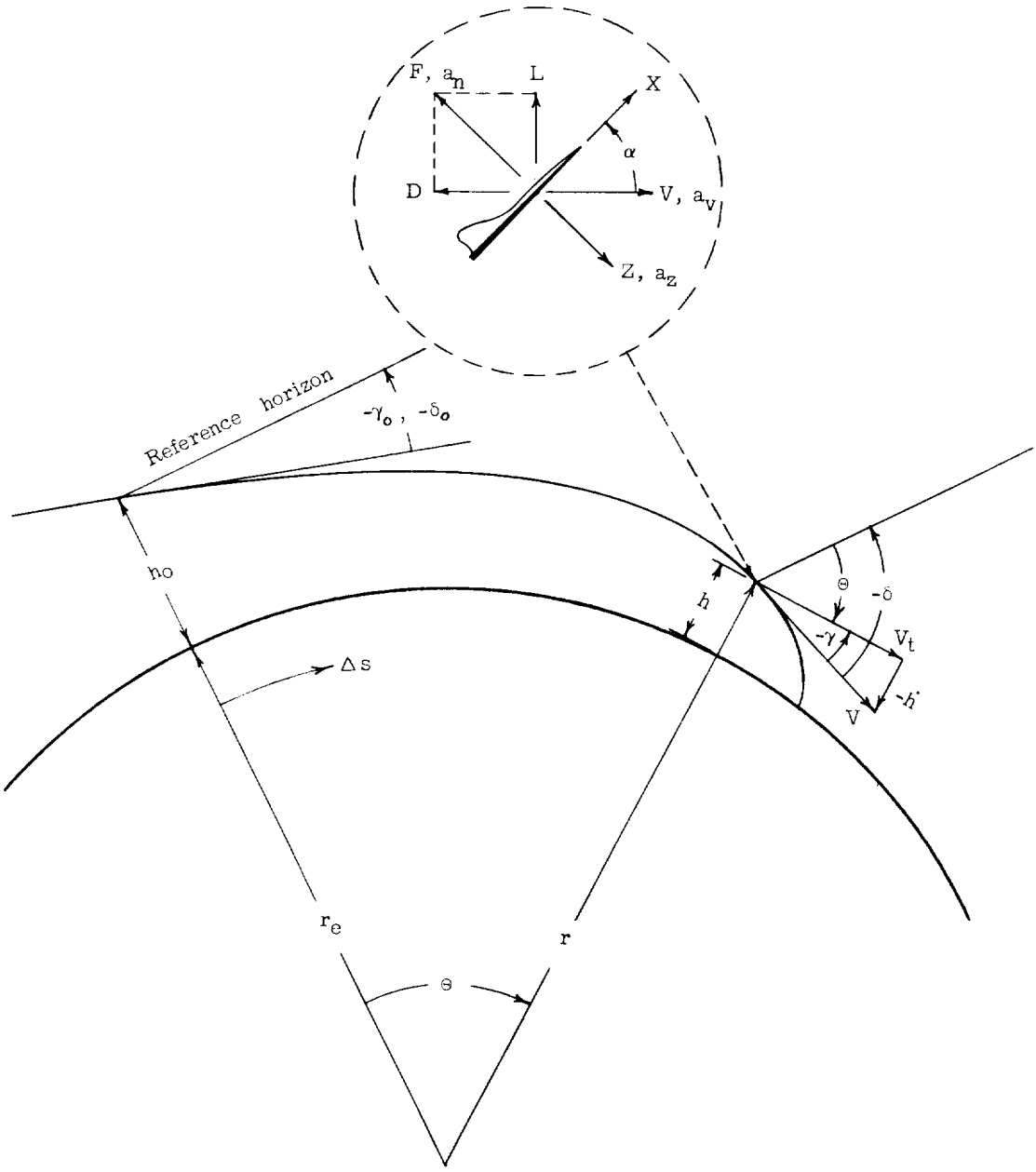

Figure 1.- Pictorial description of an entry trajectory showing trajectory variables, aerodynamic forces, and vehicle axis system. Unless denoted as negative, arrowheads indicate direction of positive displacements.

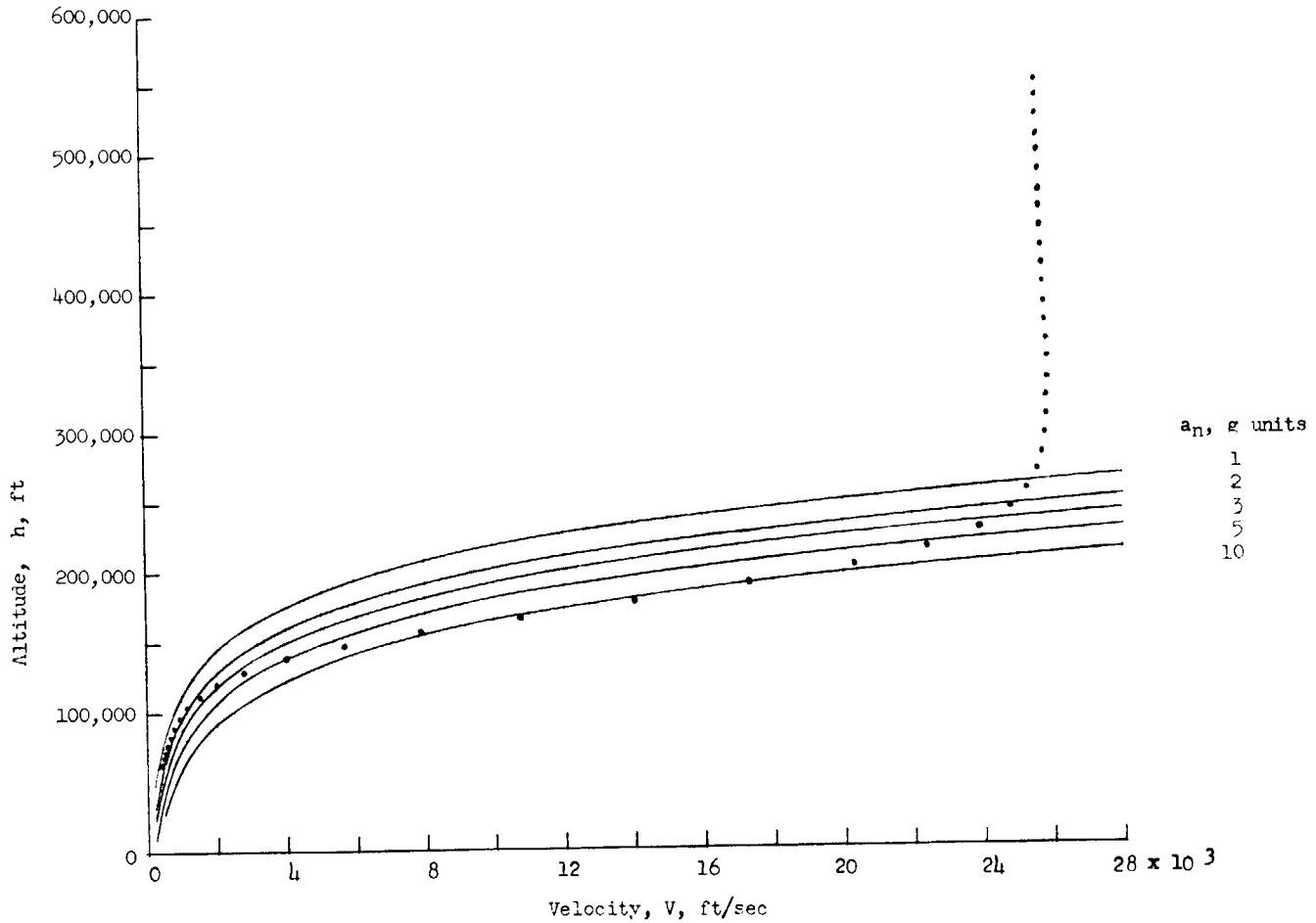

Figure 2.- Variation of altitude with velocity necessary to maintain a constant value of deceleration a_n. Superimposed with dots is the altitude-velocity variation for a typical nonlifting trajectory. Time spacing between dots is 10 seconds. Conditions at initial dot: h_o = 551,313 feet, V_o = 25,633 feet per second, γ_o = 2.96°.

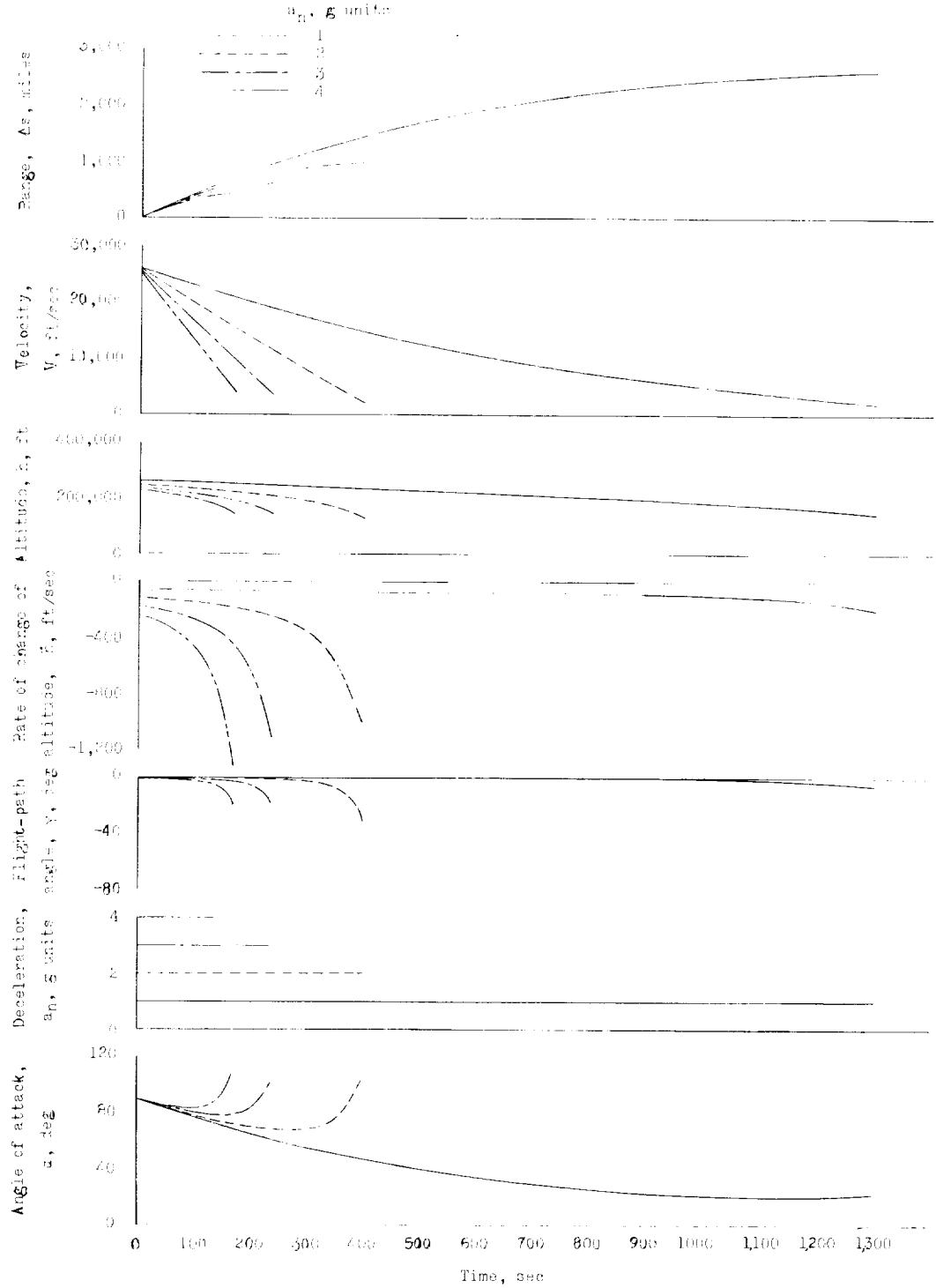

Figure 3.- Trajectory data for entry into the earth's atmosphere at a constant value of deceleration. Time histories are shown for decelerations of 1g, 2g, 3g, and 4g. In each case, $\alpha_o = 90^o$.

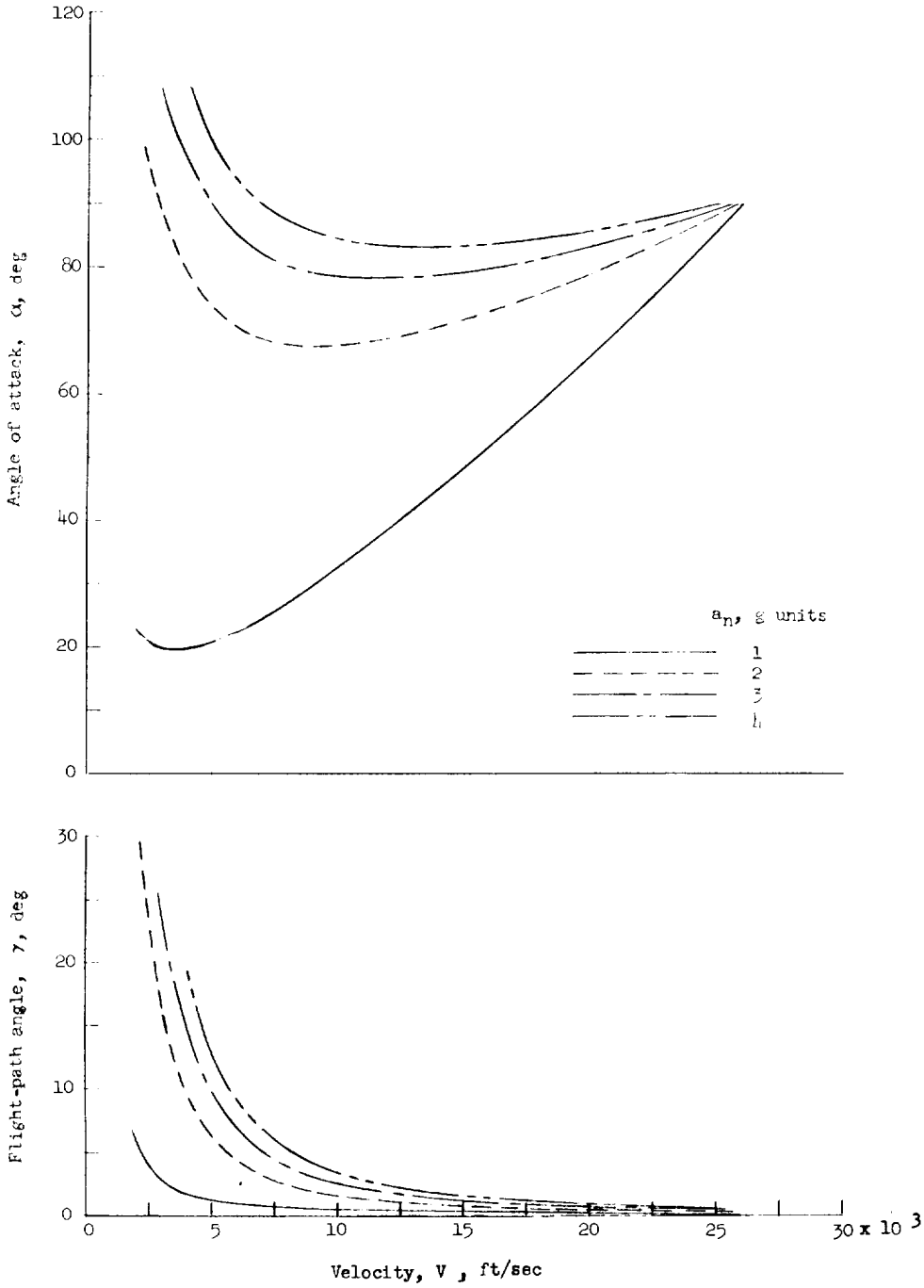

Figure 4.- The variation with velocity of angle of attack and flight-path angle for constant-deceleration trajectories. Variations and magnitudes are independent of C_F and W/S.

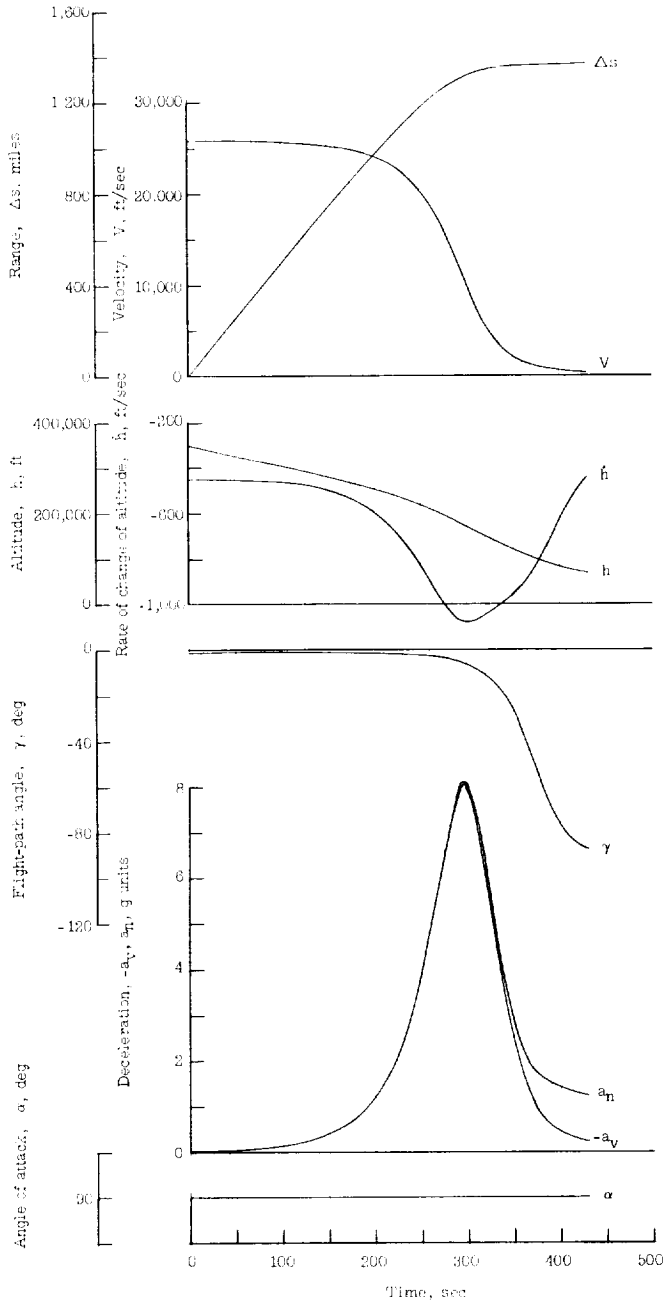

(a) Nonlifting; $\alpha = \alpha_o = 90^o$.

Figure 5.- Time histories of entry trajectories for nonlifting and controlled lift cases. V_o = 25,863 feet per second, h_o = 350,000 feet, $\gamma_o = -1^o$.

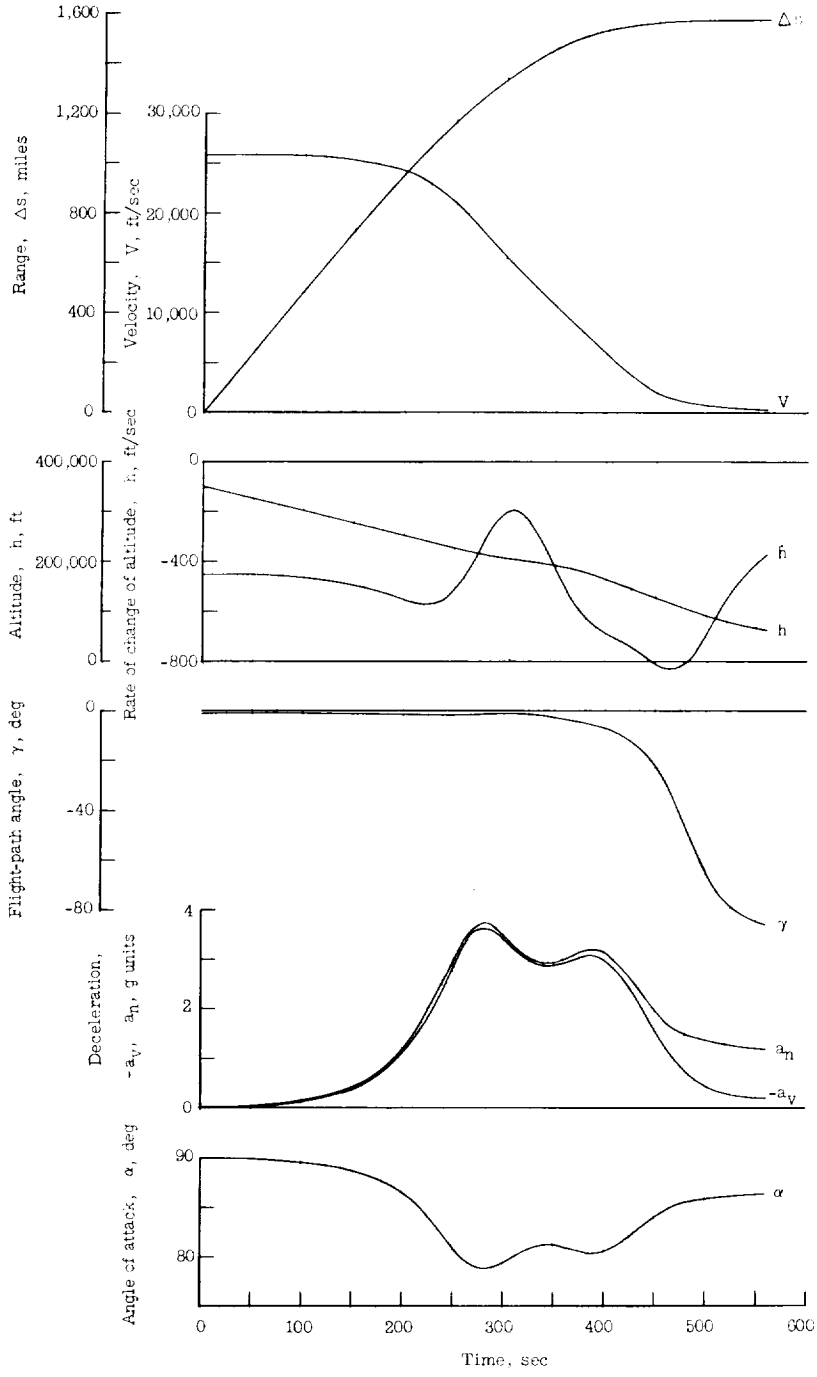

(b) Controlled lift; $\alpha = 90^{\circ} - 3a_n$.

Figure 5.- Concluded.

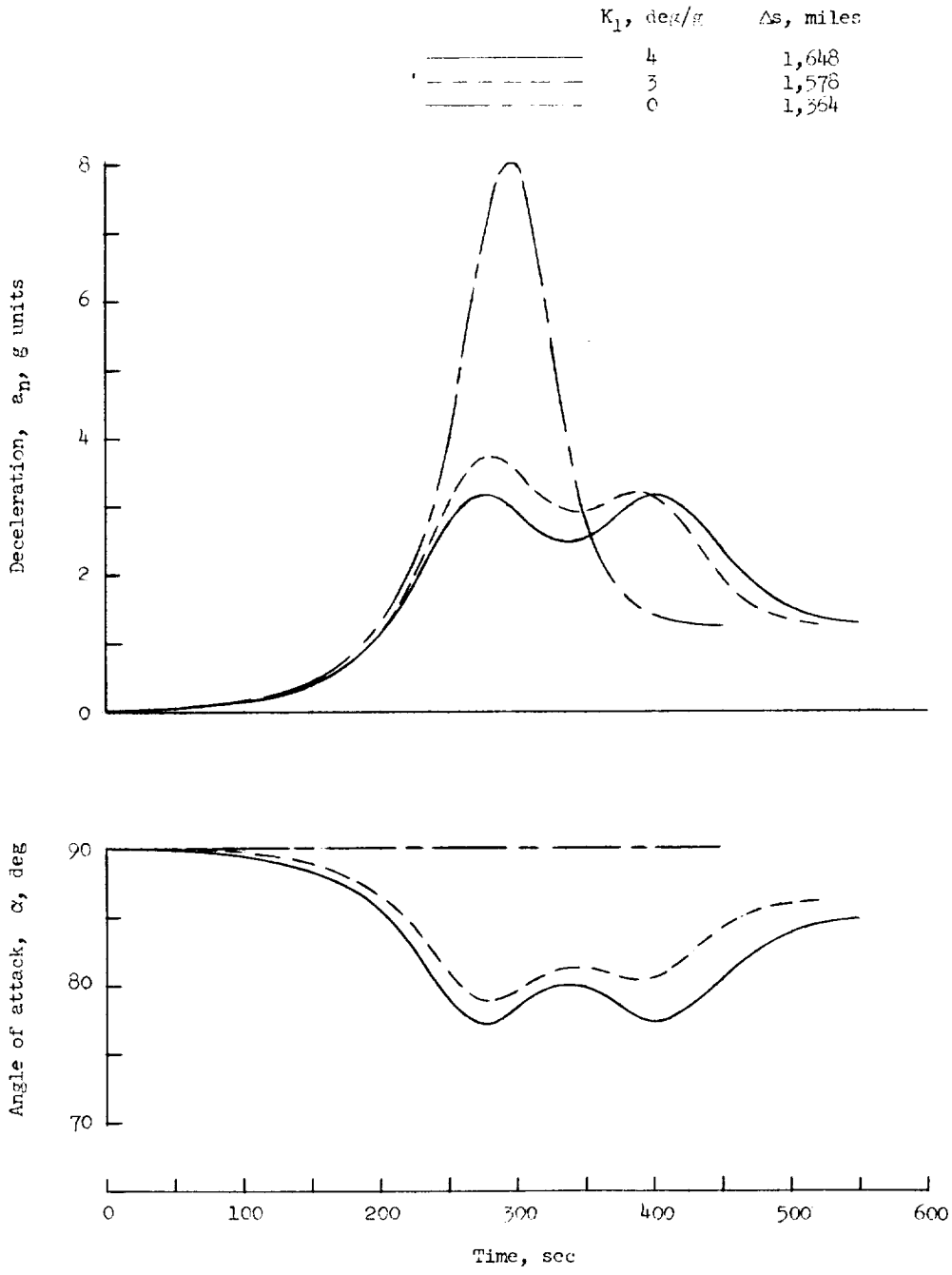

Figure 6.- Comparison of trajectories controlled with $\alpha = 90^\circ - K_1 a_n$ when K_1 has values of 0, 3, and 4 deg/g. V_o = 25,863 feet per second; h_o = 350,000 feet; $\gamma_o = -1^\circ$.

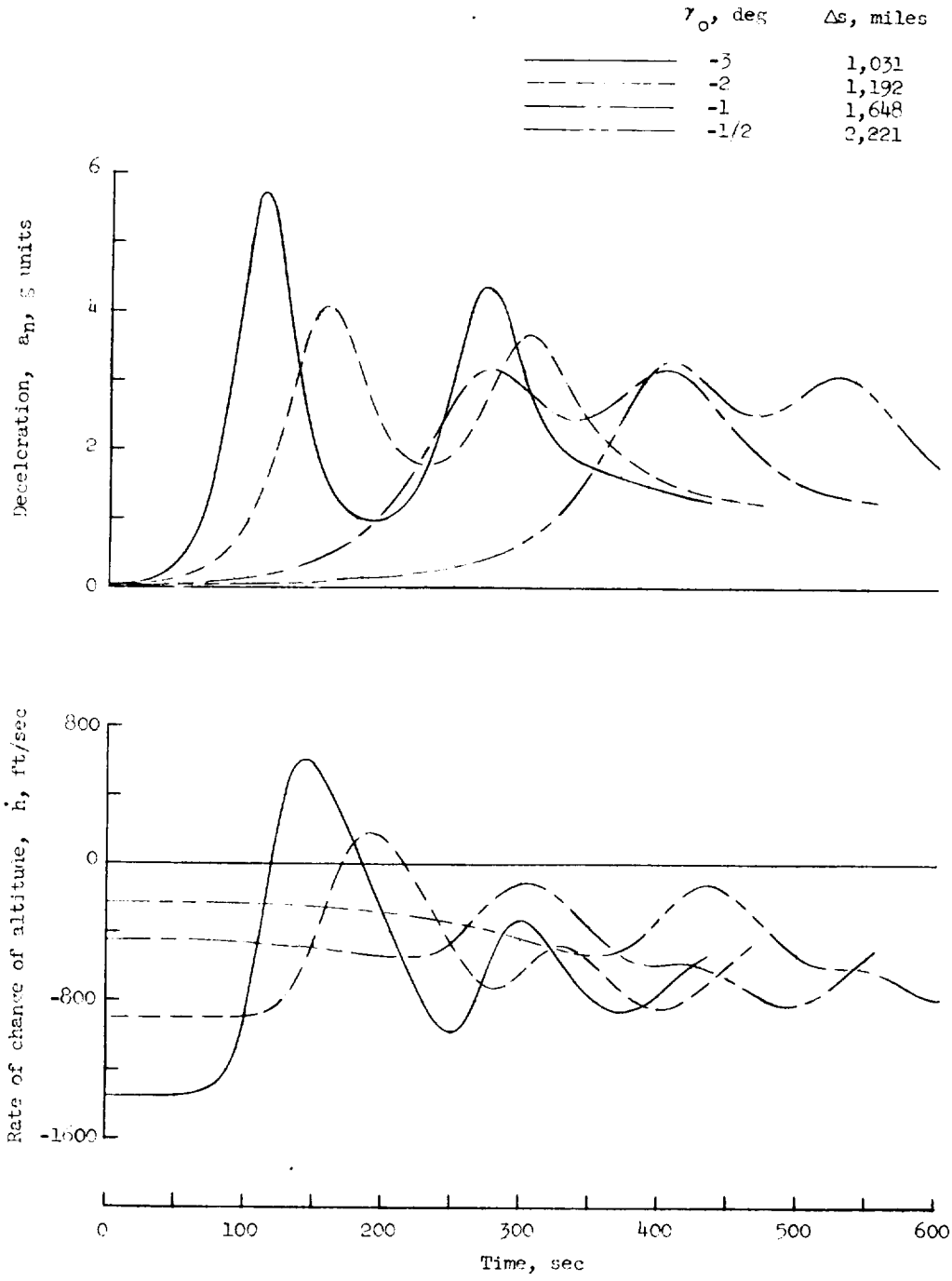

Figure 7.- Comparison of trajectories controlled with $\alpha = 90^\circ - 4a_n$ when initial flight-path angles are $-\frac{1}{2}^\circ$, -1°, -2°, and -3°. V_o = 25,863 feet per second; h_o = 350,000 feet.

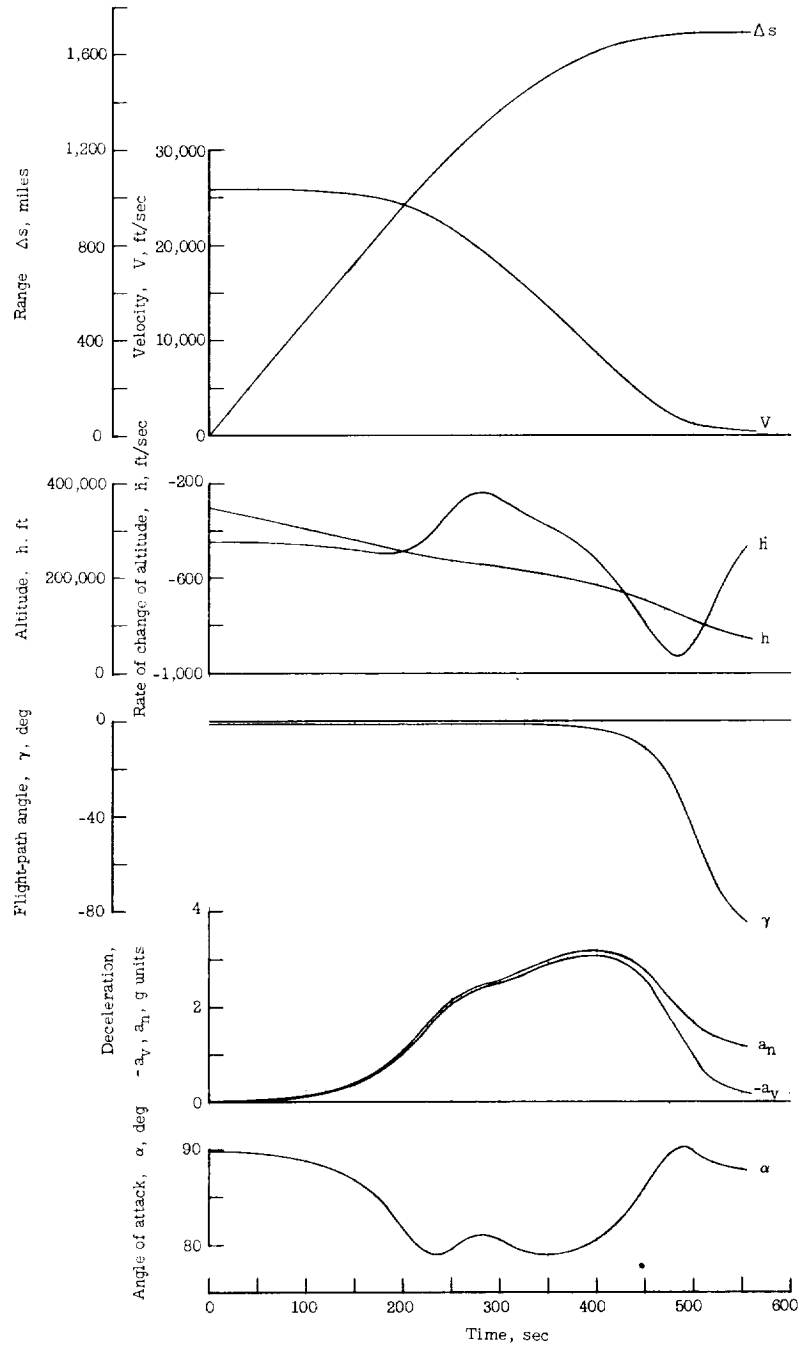

Figure 8.- Time history of entry trajectory controlled with $\alpha = 90^{\circ} - 3a_n - 250\dot{a}_n$. V_o = 25,863 feet per second; h_o = 350,000 feet; $\gamma_o = -1^{\circ}$.

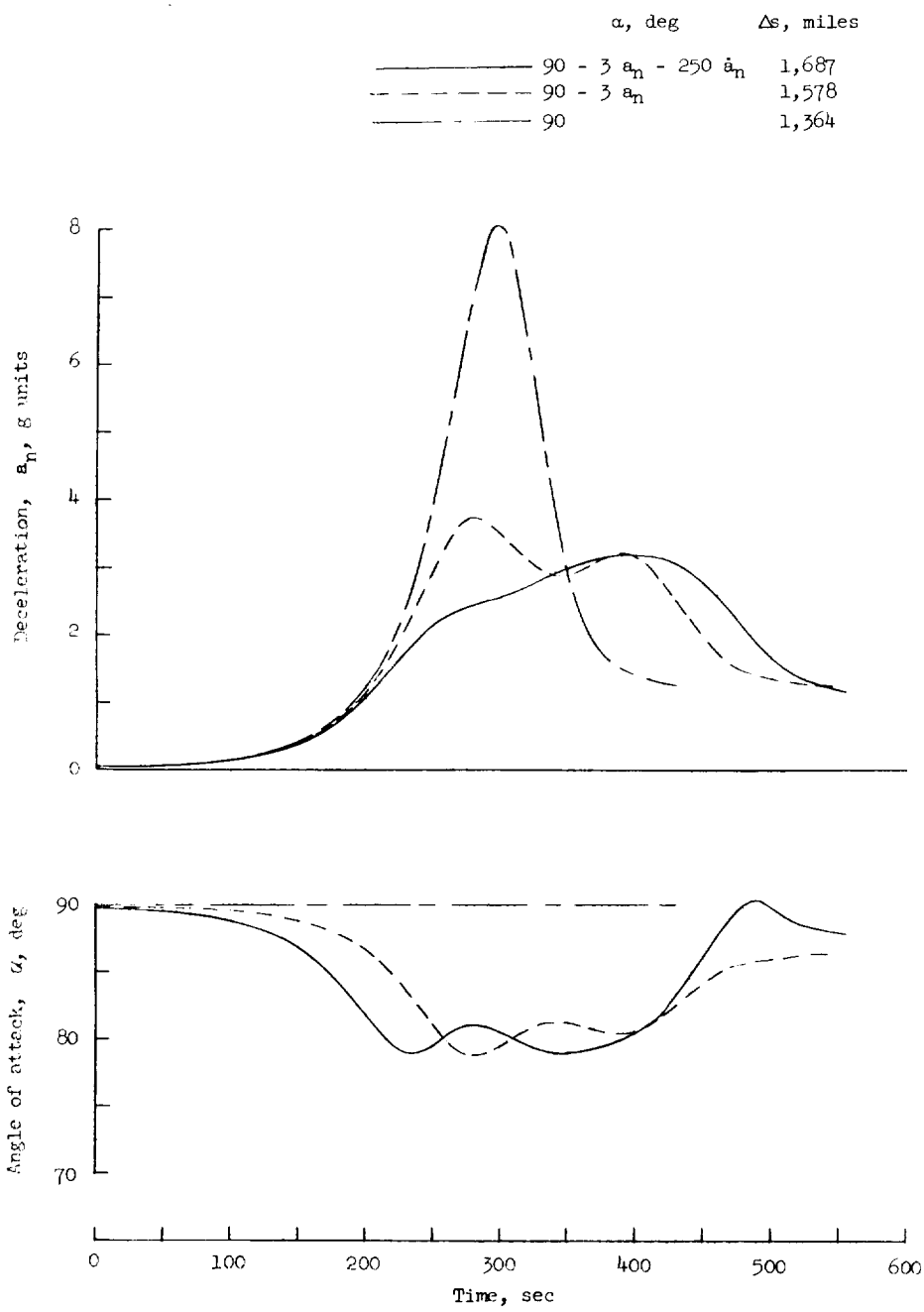

Figure 9.- Comparison of a trajectory controlled as a function of a_n and $\dot{a}_n$ with a trajectory controlled as a function of a_n only and a trajectory made at zero lift. V_o = 25,863 feet per second; h_o = 350,000 feet; γ_o = -1°.

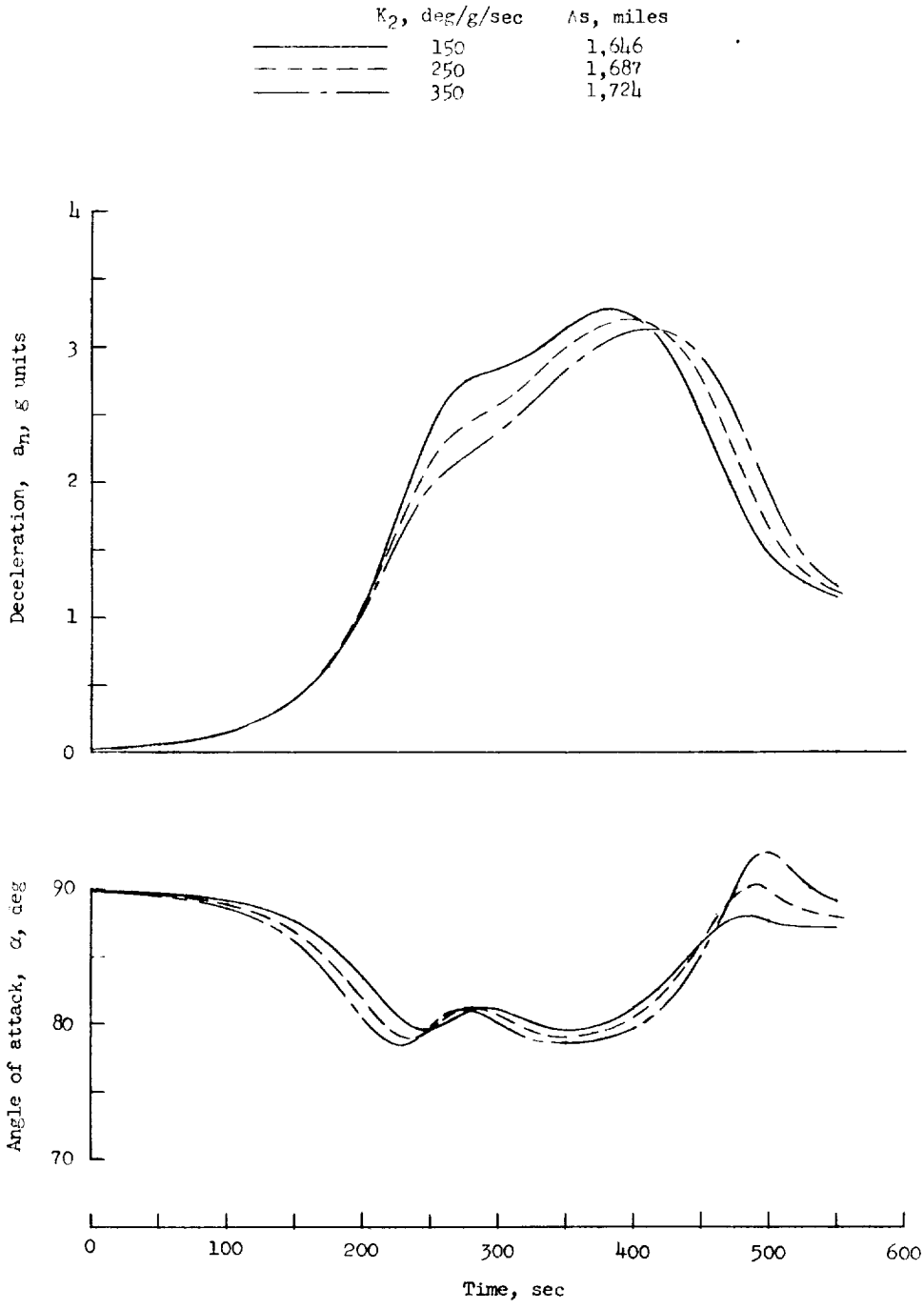

Figure 10.- Comparison of trajectories controlled with $\alpha = 90 - 3a_n - K_2\dot{a}_n$ when K_2 has the values 150, 250, and 350 degrees/g/second. V_o = 25,863 feet per second; h_o = 350,000 feet; $\gamma_o = -1^o$.

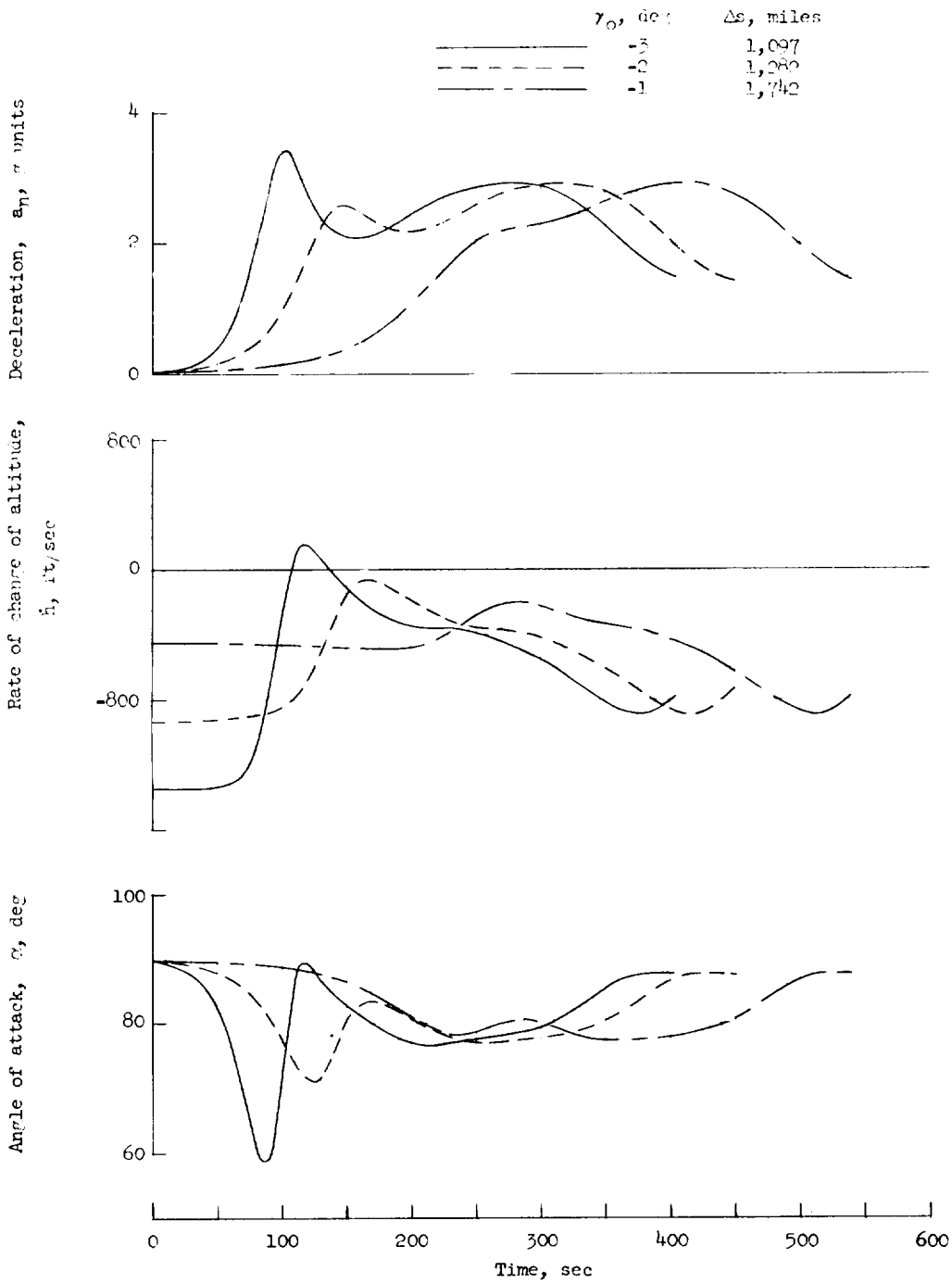

Figure 11.- Comparison of trajectories controlled with $\alpha = 90 - 4a_n - 250\dot{a}_n$ with initial flight-path angles are -1°, -2°, and -3°. V_o = 25,863 feet per second; h_o = 350,000 feet.

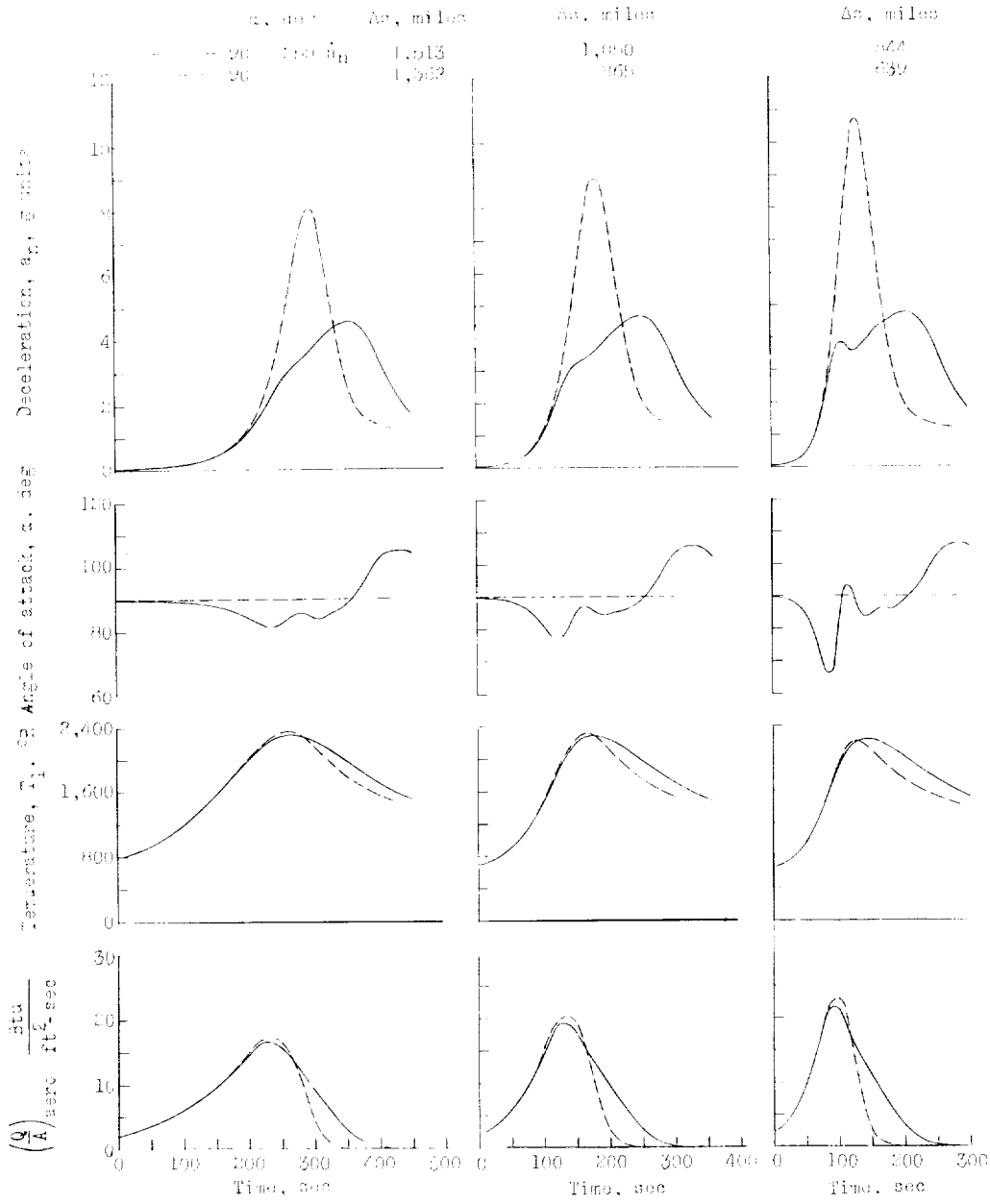

(a) $\gamma_o = -1^o$. (b) $\gamma_o = -2^o$. (c) $\gamma_o = -3^o$.

Figure 12.- Comparison of trajectory data, skin temperatures, and aerodynamic heat-transfer rates for initial flight-path angles of -1^o, -2^o, and -3^o when trajectory is controlled with $\alpha = 90^o$ = Constant and $\alpha = 90^o = 250\dot{a}_n$. V_o = 25,863 feet per second; h_o = 350,000 feet.

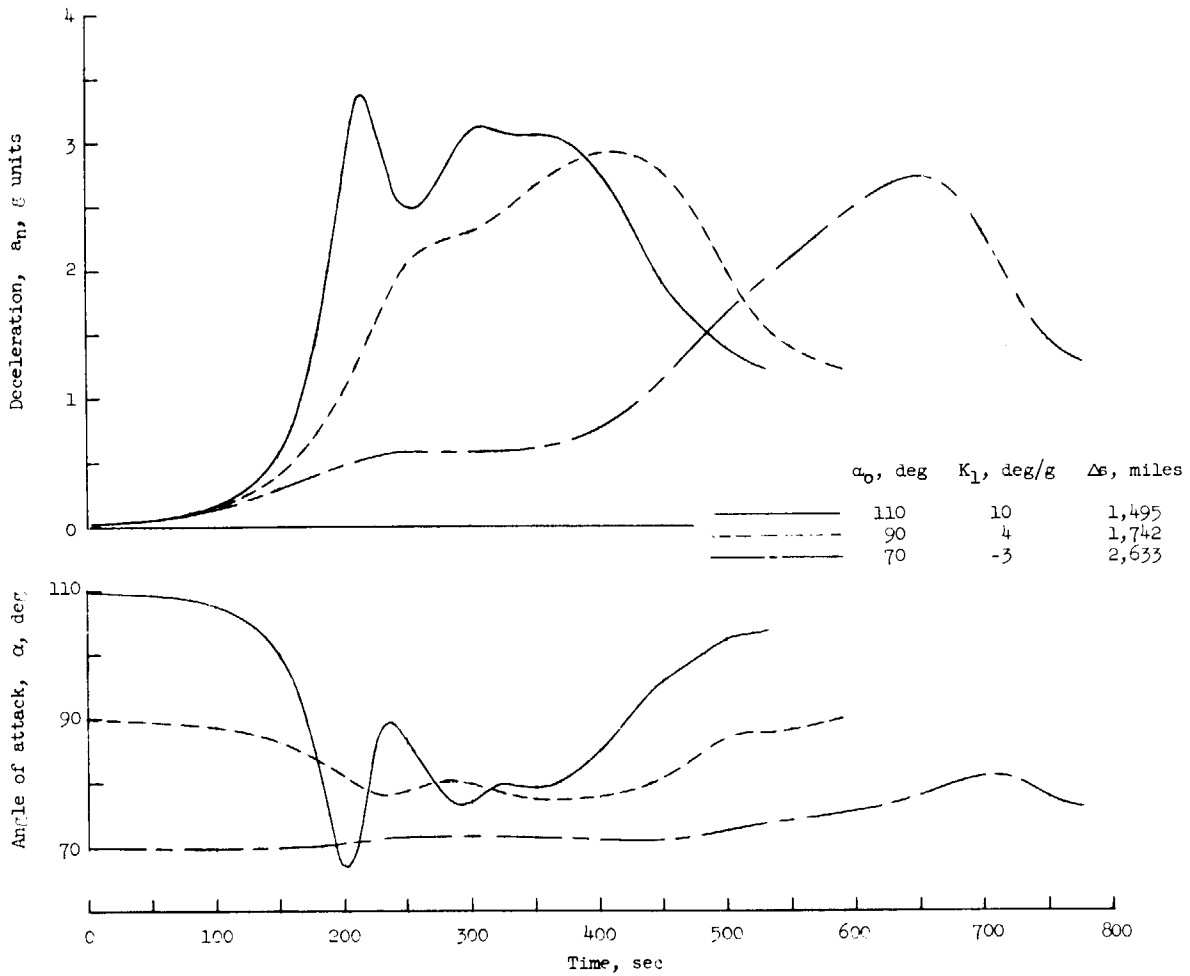

Figure 13.- Comparison of trajectories controlled with $\alpha = \alpha_o - K_1 a_n - 250\dot{a}_n$ when initial angle of attack is 110°, 90°, and 70° and the gain of K_1 is a function of this initial angle of attack. $\gamma_o = -1°$; $V_o = 25{,}863$ feet per second; $h_o = 350{,}000$ feet.

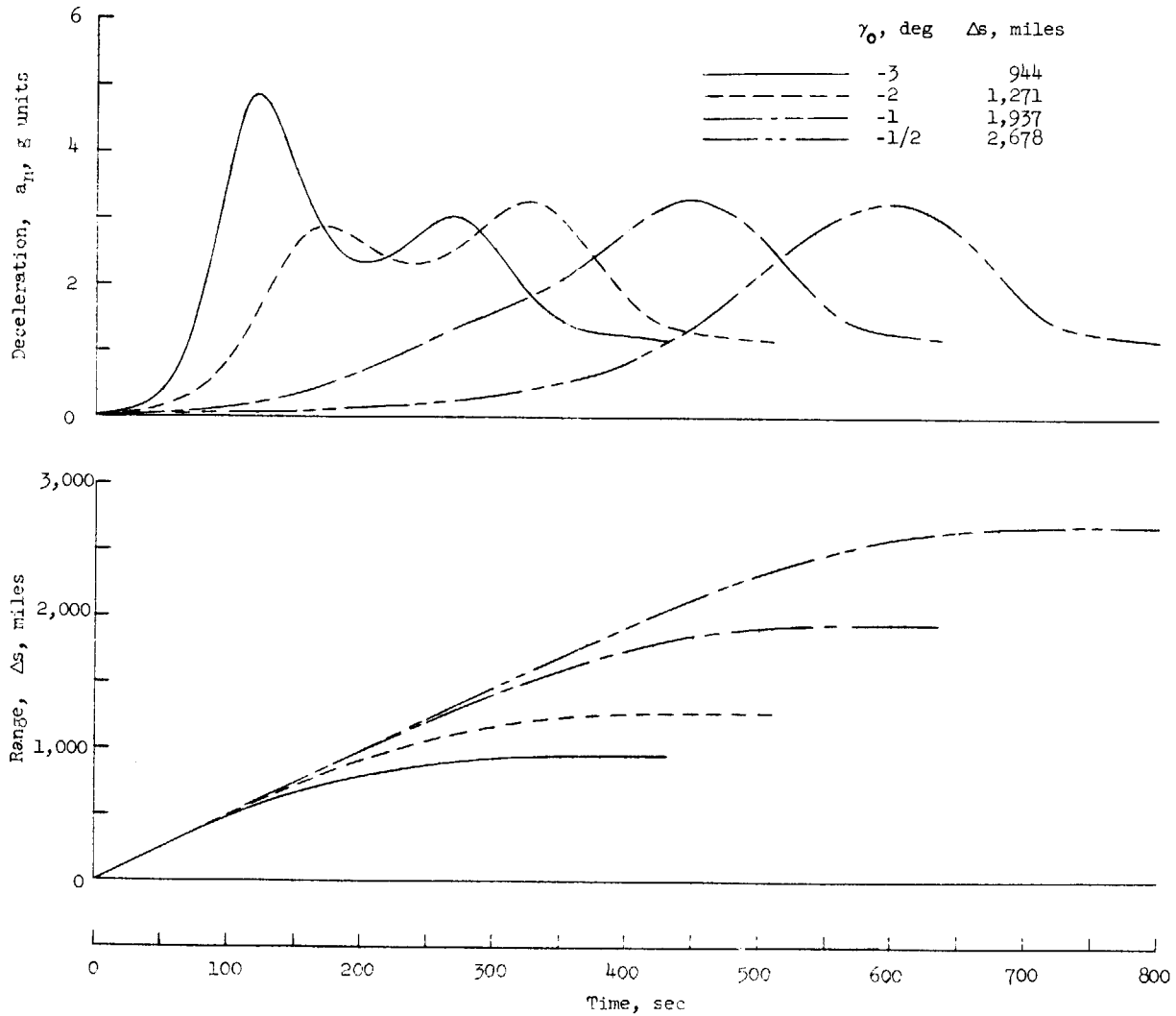

Figure 14.- Comparison of trajectories when angle of attack is held constant at 79°. Initial flight-path angles are $-\frac{1}{2}^\circ$, -1°, -2°, and -3°. V_o = 25,863 feet per second; h_o = 350,000 feet.

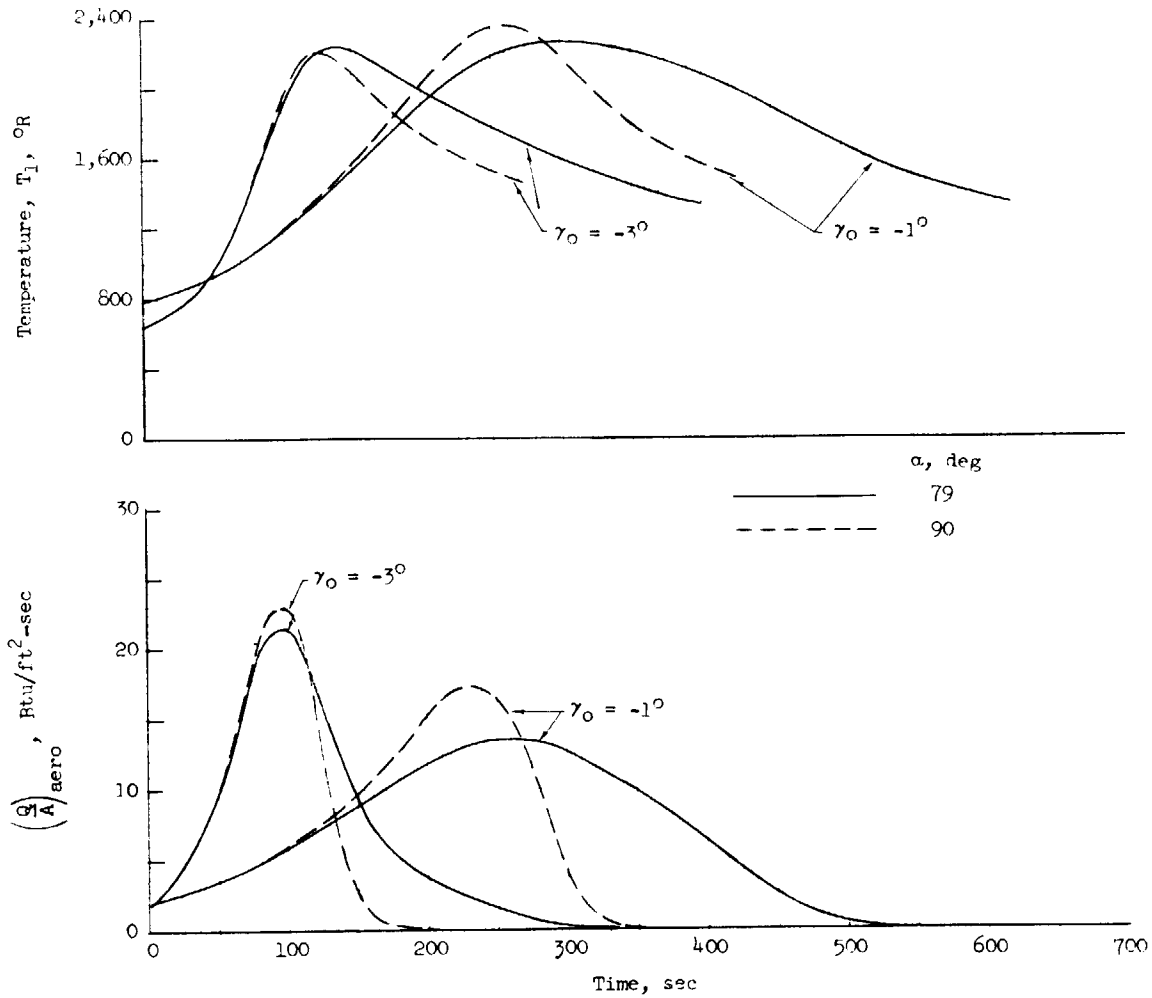

Figure 15.- Comparison of skin temperatures and aerodynamic heat-transfer rates when angle of attack is held constant at 90° and 79°. Data are shown for initial flight-path angles of -1 and -3°. V_o = 25,863 feet per second; h_o = 350,000 feet.

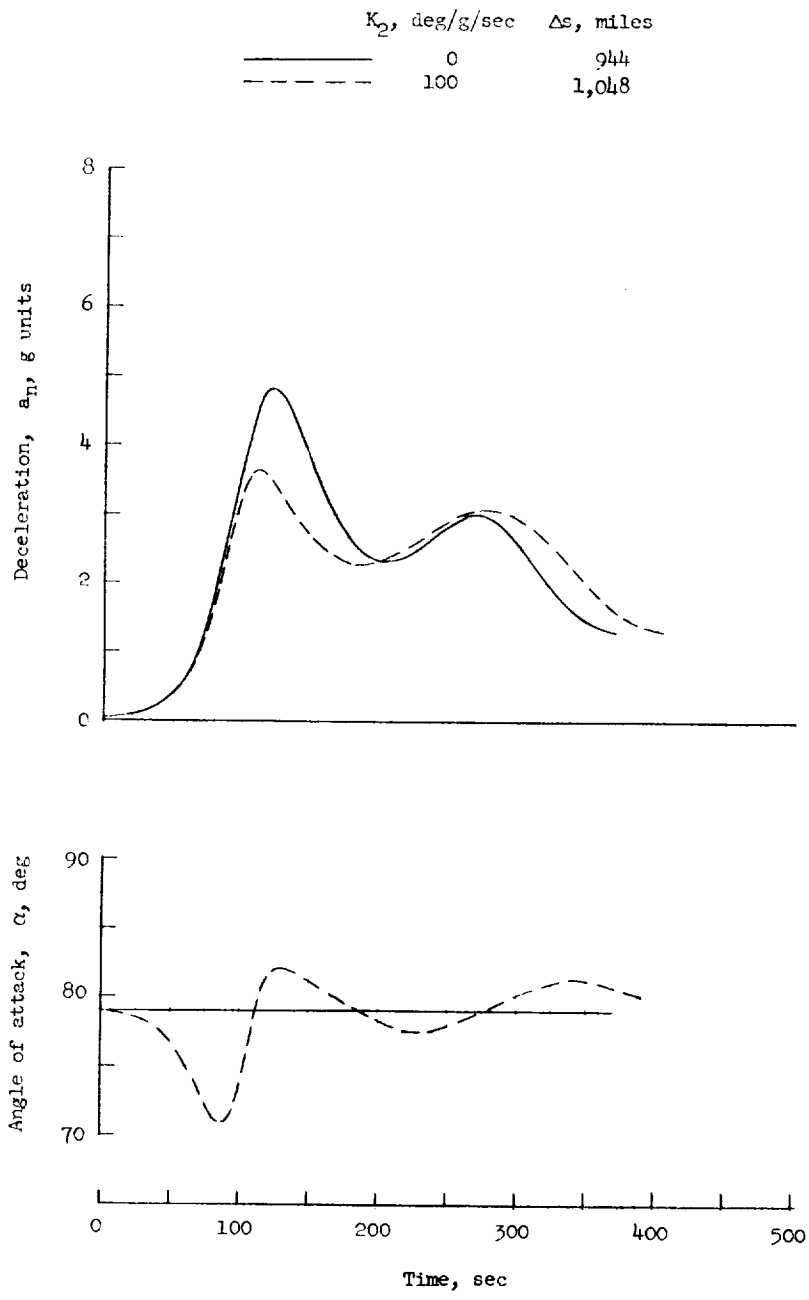

(a) $\alpha_o = 79^\circ$.

Figure 16.- Comparison of trajectories made with $\alpha = \alpha_o - K_2\dot{a}_n$ where K_2 is 100 degree/g/second and zero (constant α). $\gamma_o = -3^\circ$; V_o = 25,863 feet per second; h_o = 350,000 feet.

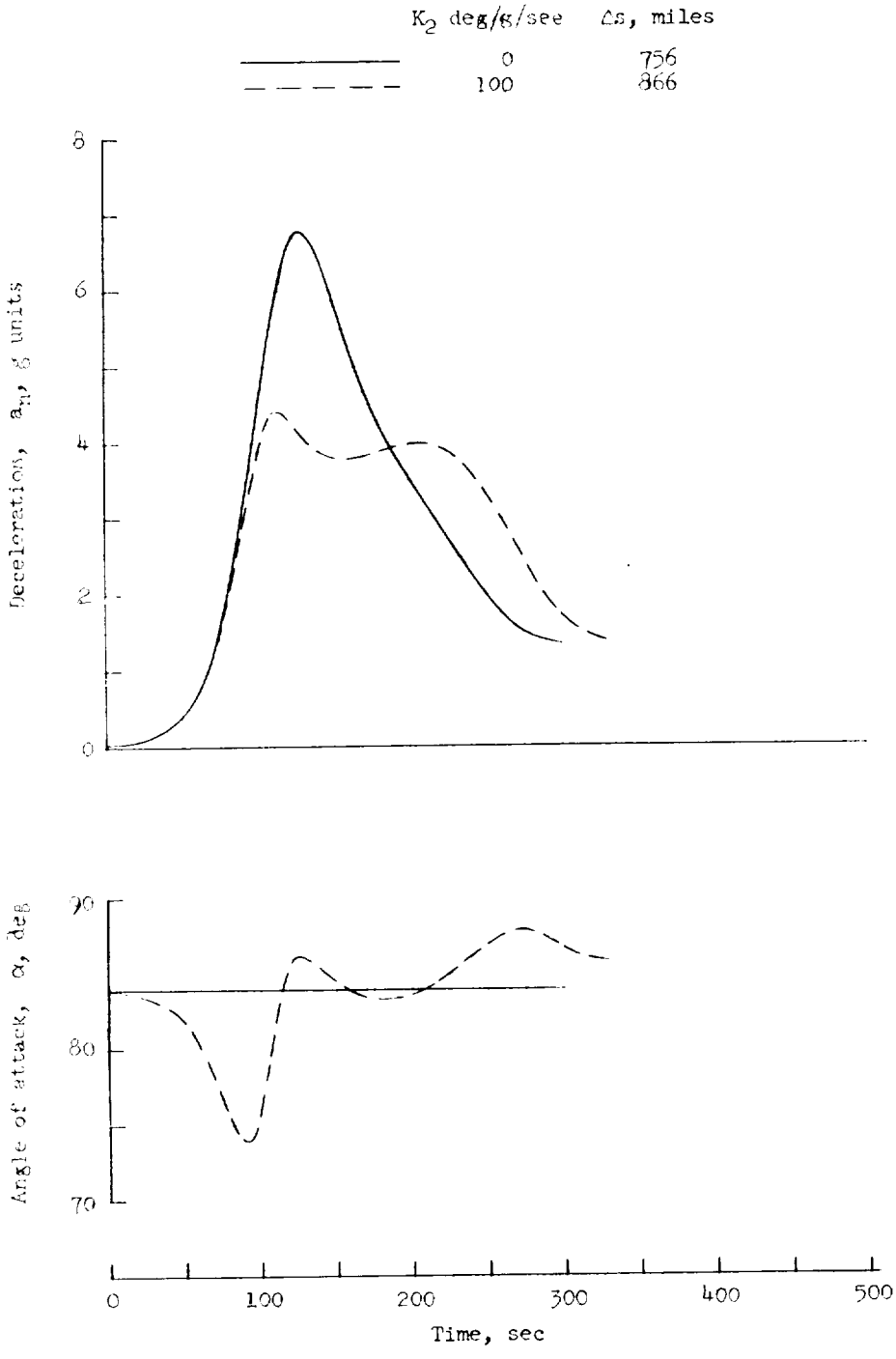

(b) $\alpha_o = 84^o$.

Figure 16.- Concluded.

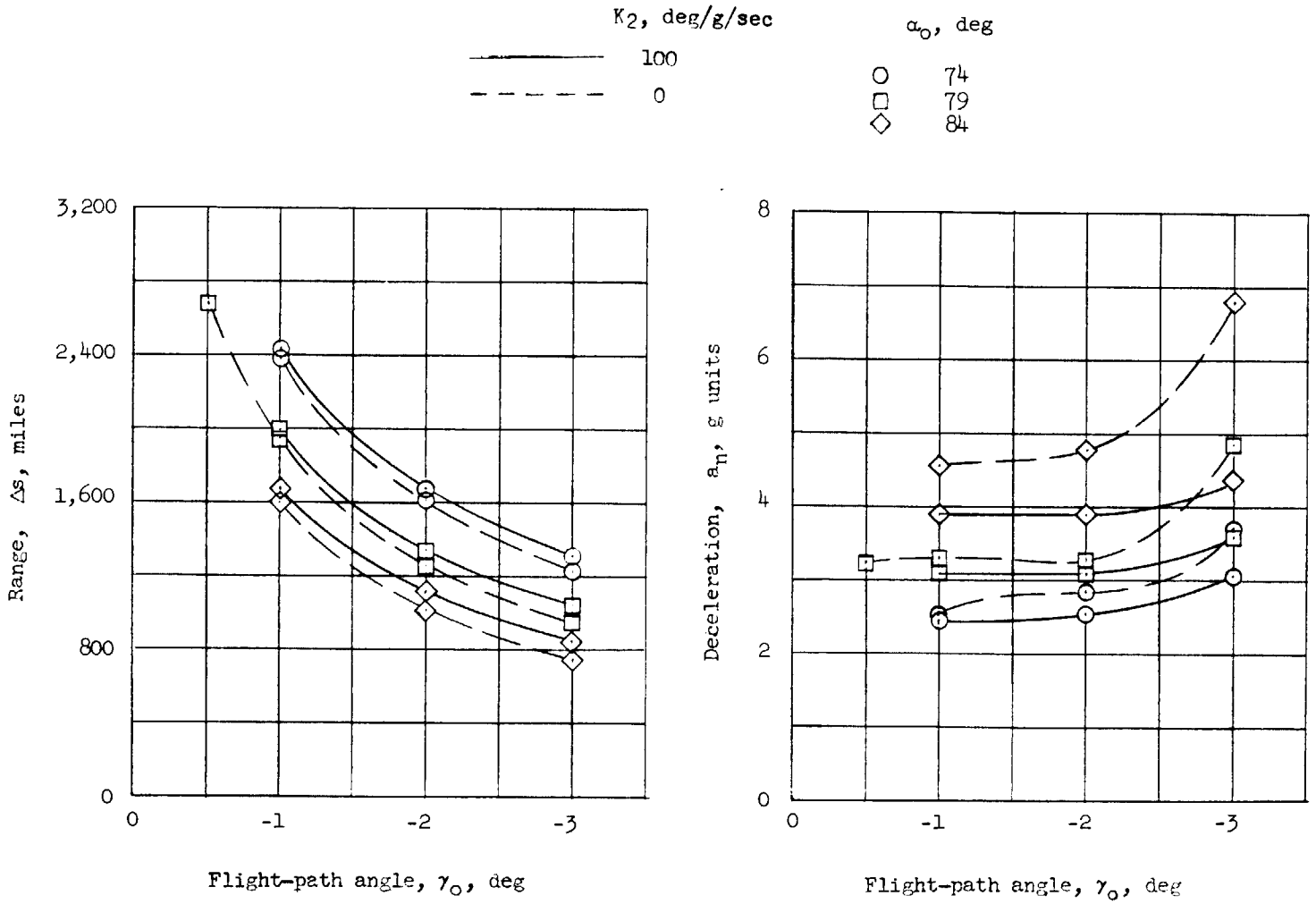

Figure 17.- Range and maximum decelerations as a function of the initial flight-path angle obtained from entry trajectories where the lift-drag ratio was controlled by $\alpha = \alpha_o - K_2\dot{a}_n$. V_o = 25,863 feet per second; h_o = 350,000 feet.

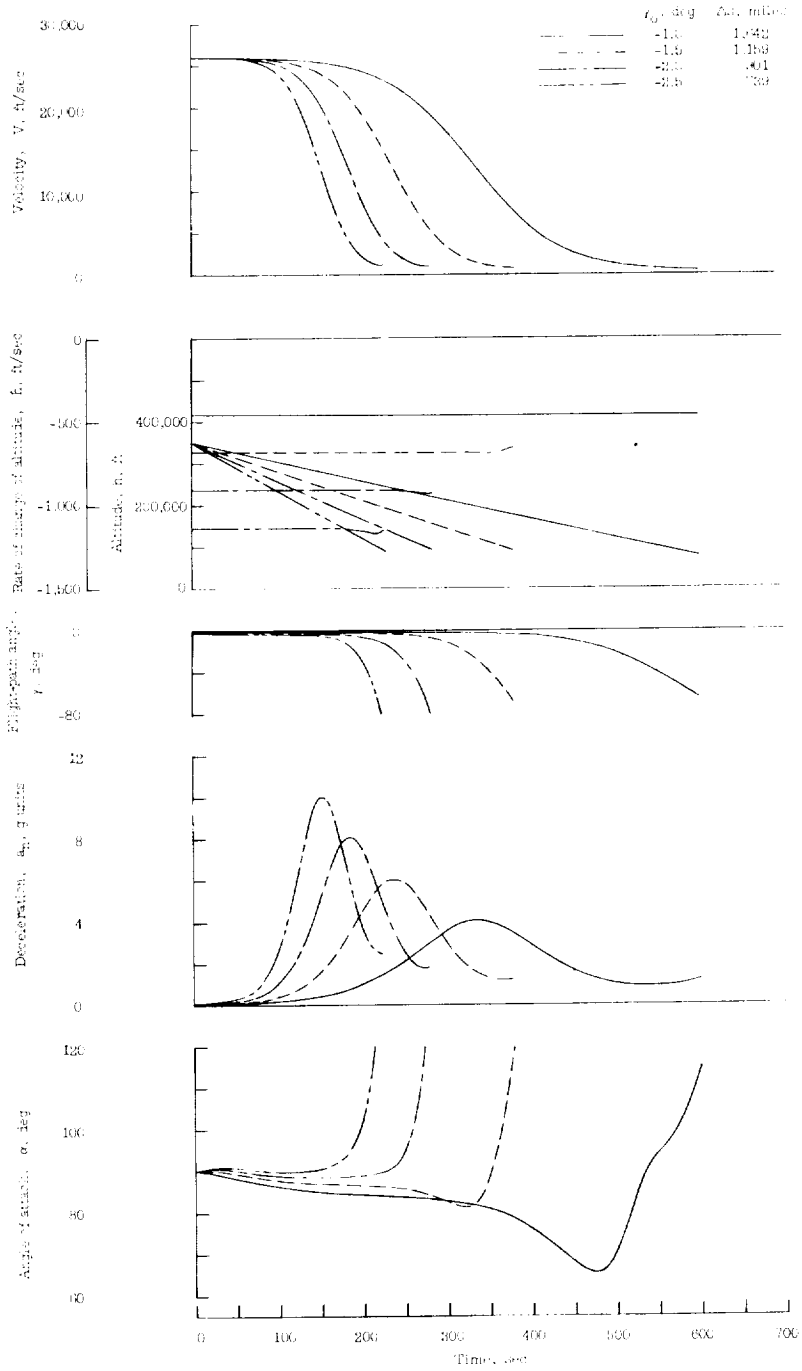

Figure 18.- Trajectory data for entry into the earth's atmosphere at a constant rate of descent. Rates of descent determined from initial flight-path angles; V_o = 26,000 feet per second; h_o = 350,000 feet.

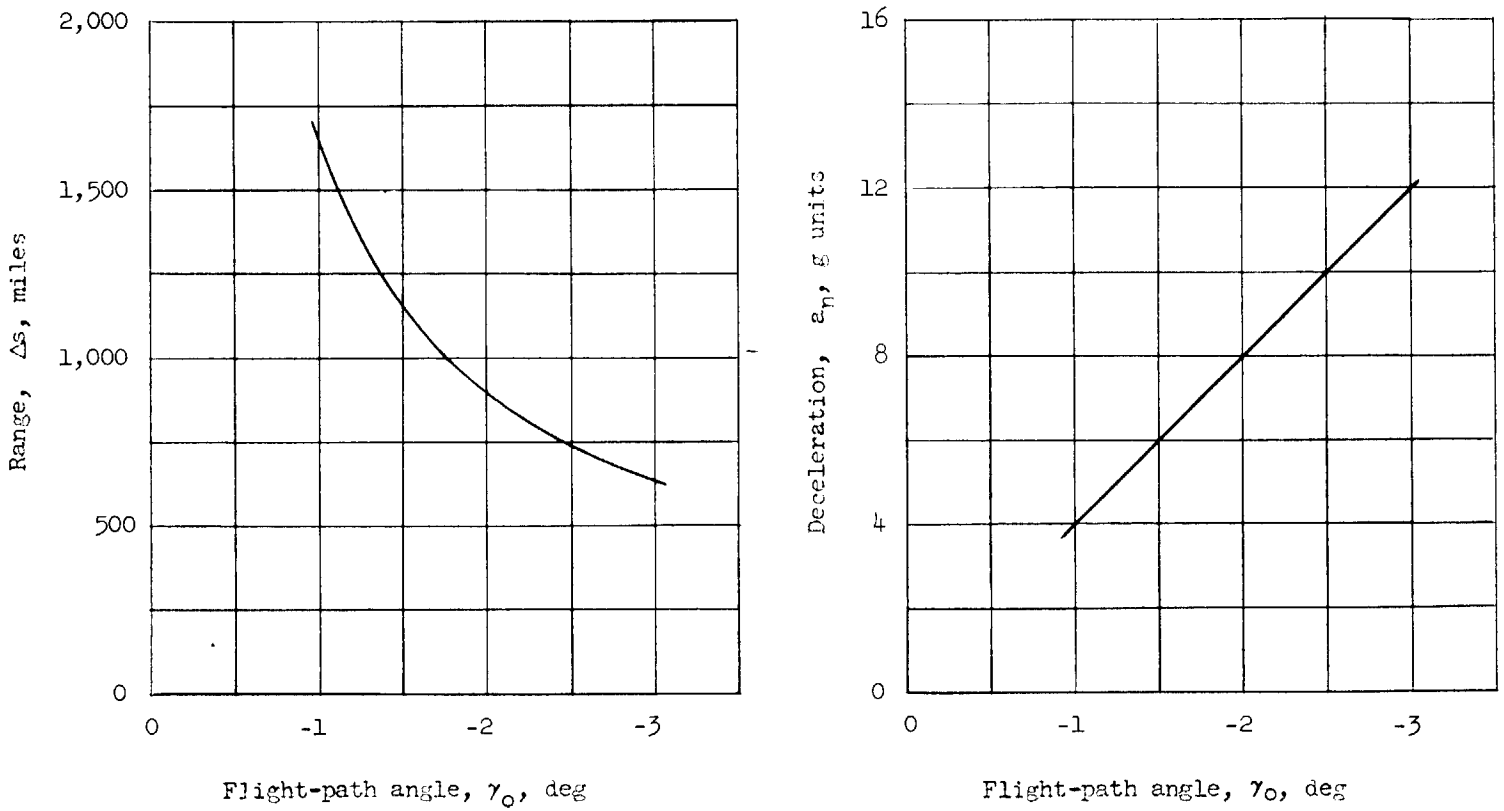

Figure 19.- Range and maximum deceleration as a function of the initial flight-path angle obtained from atmospheric entries made at constant rates of descent. V_o = 26,000 feet per second; h_o = 350,000 feet.

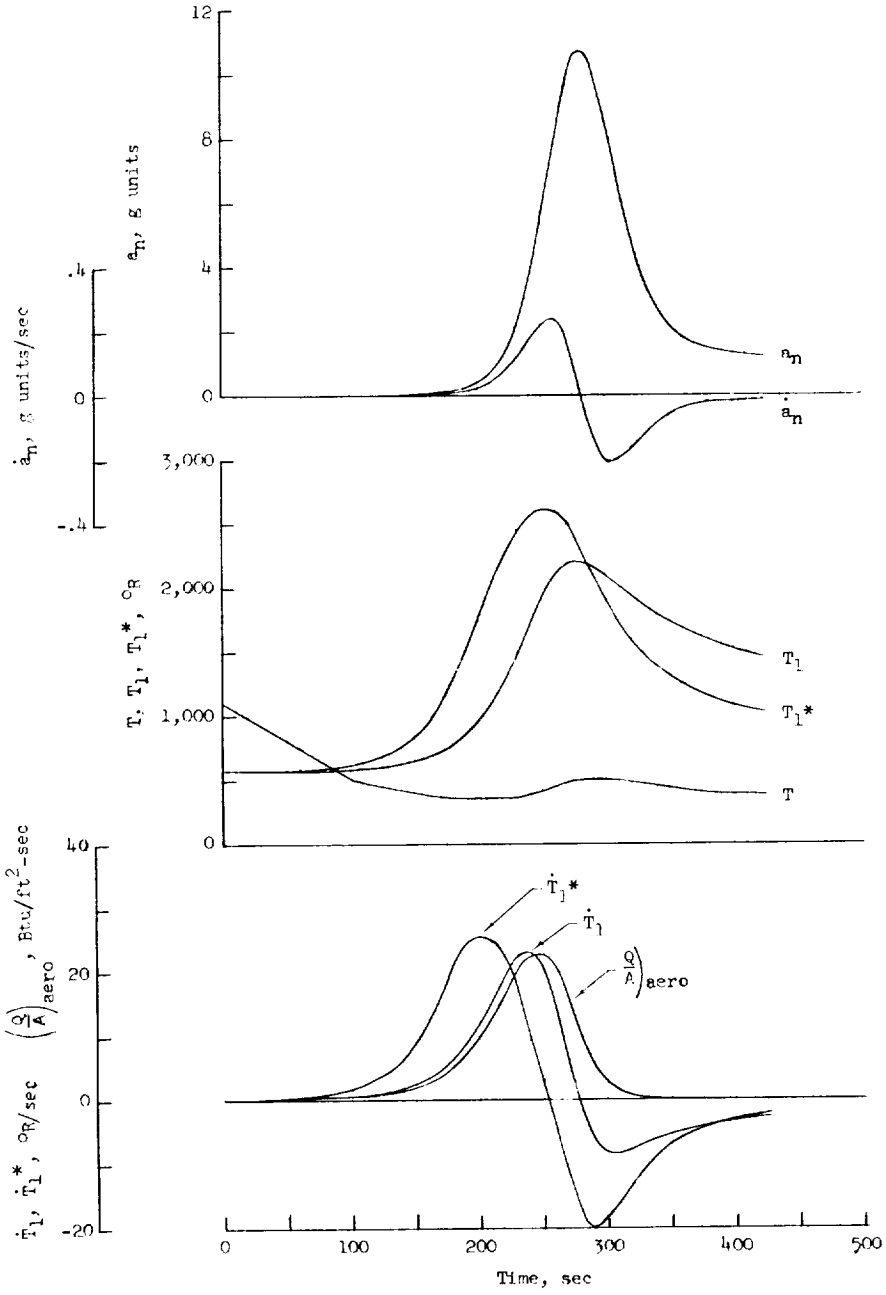

Figure 20.- Comparison of deceleration temperature and aerodynamic-heating data calculated for a typical atmospheric entry. h_o = 551,313.5 feet; V_o = 25,633.5 feet per second; γ_o = -2.96°. (At 150 seconds, h = 350,000 feet; V = 25,863 feet per second; and γ_o = -3.0°.)

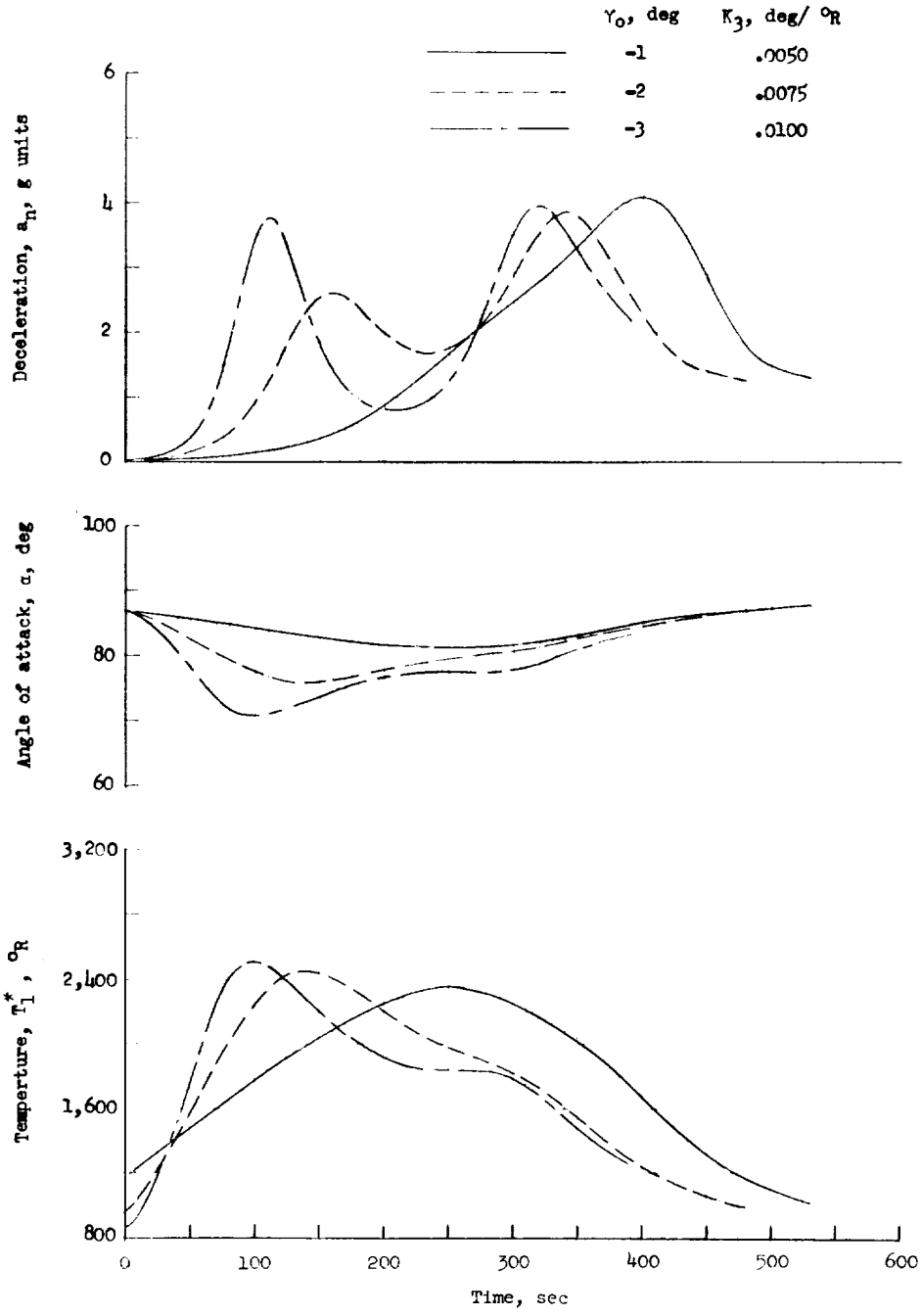

Figure 21.- Comparison of trajectories controlled with $\alpha = 90^\circ - K_3\left[T_1^* - (T_1^*)_{550,000}\right]$ when initial flight-path angles are -1°, -2°, and -3°. V_o = 25,863 feet per second; h_o = 350,000 feet.

NASA MEMO 1-19-59L
National Aeronautics and Space Administration.
TRAJECTORY CONTROL FOR VEHICLES ENTERING THE EARTH'S ATMOSPHERE AT SMALL FLIGHT-PATH ANGLES. John M. Eggleston and John W. Young. February 1959. 64p. diagrs.
(NASA MEMORANDUM 1-19-59L)
(Title, Unclassified)

Methods of controlling the trajectories of high-drag—low-lift vehicles entering the earth's atmosphere at angles of attack near 90° and at initial entry angles up to 3° are studied. The trajectories are calculated for vehicles whose angle of attack can be held constant at some specified value or can be perfectly controlled as a function of some measured quantity along the trajectory. The results might be applied in the design of automatic control systems or in the design of instruments which will give the human pilot sufficient information to control his trajectory properly during an atmospheric entry. Trajectory data are compared on the basis of the deceleration, range, angle of

Copies obtainable from NASA, Washington (over)

1. Aerodynamics With Heat (1.1.4)
2. Control (1.8.2)
3. Stabilization, Automatic (1.8.8)

I. Eggleston, John M.
II. Young, John W.
III. NASA MEMO 1-19-59L

NASA

NASA MEMO 1-19-59L
National Aeronautics and Space Administration.
TRAJECTORY CONTROL FOR VEHICLES ENTERING THE EARTH'S ATMOSPHERE AT SMALL FLIGHT-PATH ANGLES. John M. Eggleston and John W. Young. February 1959. 64p. diagrs.
(NASA MEMORANDUM 1-19-59L)
(Title, Unclassified)

Methods of controlling the trajectories of high-drag—low-lift vehicles entering the earth's atmosphere at angles of attack near 90° and at initial entry angles up to 3° are studied. The trajectories are calculated for vehicles whose angle of attack can be held constant at some specified value or can be perfectly controlled as a function of some measured quantity along the trajectory. The results might be applied in the design of automatic control systems or in the design of instruments which will give the human pilot sufficient information to control his trajectory properly during an atmospheric entry. Trajectory data are compared on the basis of the deceleration, range, angle of

Copies obtainable from NASA, Washington (over)

1. Aerodynamics With Heat (1.1.4)
2. Control (1.8.2)
3. Stabilization, Automatic (1.8.8)

I. Eggleston, John M.
II. Young, John W.
III. NASA MEMO 1-19-59L

NASA

NASA MEMO 1-19-59L
National Aeronautics and Space Administration.
TRAJECTORY CONTROL FOR VEHICLES ENTERING THE EARTH'S ATMOSPHERE AT SMALL FLIGHT-PATH ANGLES. John M. Eggleston and John W. Young. February 1959. 64p. diagrs.
(NASA MEMORANDUM 1-19-59L)
(Title, Unclassified)

Methods of controlling the trajectories of high-drag—low-lift vehicles entering the earth's atmosphere at angles of attack near 90° and at initial entry angles up to 3° are studied. The trajectories are calculated for vehicles whose angle of attack can be held constant at some specified value or can be perfectly controlled as a function of some measured quantity along the trajectory. The results might be applied in the design of automatic control systems or in the design of instruments which will give the human pilot sufficient information to control his trajectory properly during an atmospheric entry. Trajectory data are compared on the basis of the deceleration, range, angle of

Copies obtainable from NASA, Washington (over)

1. Aerodynamics With Heat (1.1.4)
2. Control (1.8.2)
3. Stabilization, Automatic (1.8.8)

I. Eggleston, John M.
II. Young, John W.
III. NASA MEMO 1-19-59L

NASA

NASA MEMO 1-19-59L
National Aeronautics and Space Administration.
TRAJECTORY CONTROL FOR VEHICLES ENTERING THE EARTH'S ATMOSPHERE AT SMALL FLIGHT-PATH ANGLES. John M. Eggleston and John W. Young. February 1959. 64p. diagrs.
(NASA MEMORANDUM 1-19-59L)
(Title, Unclassified)

Methods of controlling the trajectories of high-drag—low-lift vehicles entering the earth's atmosphere at angles of attack near 90° and at initial entry angles up to 3° are studied. The trajectories are calculated for vehicles whose angle of attack can be held constant at some specified value or can be perfectly controlled as a function of some measured quantity along the trajectory. The results might be applied in the design of automatic control systems or in the design of instruments which will give the human pilot sufficient information to control his trajectory properly during an atmospheric entry. Trajectory data are compared on the basis of the deceleration, range, angle of

Copies obtainable from NASA, Washington (over)

1. Aerodynamics With Heat (1.1.4)
2. Control (1.8.2)
3. Stabilization, Automatic (1.8.8)

I. Eggleston, John M.
II. Young, John W.
III. NASA MEMO 1-19-59L

NASA

NASA MEMO 1-19-59L

attack, and, in some cases, the rate of descent. The aerodynamic heat-transfer rate and skin temperature of a vehicle with a simple heat-sink type of structure are calculated for trajectories made with several types of control functions.

Copies obtainable from NASA, Washington

NASA

NASA MEMO 1-19-59L

attack, and, in some cases, the rate of descent. The aerodynamic heat-transfer rate and skin temperature of a vehicle with a simple heat-sink type of structure are calculated for trajectories made with several types of control functions.

Copies obtainable from NASA, Washington

NASA

NASA MEMO 1-19-59L

attack, and, in some cases, the rate of descent. The aerodynamic heat-transfer rate and skin temperature of a vehicle with a simple heat-sink type of structure are calculated for trajectories made with several types of control functions.

Copies obtainable from NASA, Washington

NASA

NASA MEMO 1-19-59L

attack, and, in some cases, the rate of descent. The aerodynamic heat-transfer rate and skin temperature of a vehicle with a simple heat-sink type of structure are calculated for trajectories made with several types of control functions.

Copies obtainable from NASA, Washington

NASA